

UNIVERSITÀ DEGLI STUDI DI VERONA

DEPARTMENT OF MEDICINE

*GRADUATE SCHOOL OF
LIFE AND HEALTH SCIENCES*

*DOCTORAL PROGRAM IN
CLINICAL AND EXPERIMENTAL BIOMEDICAL SCIENCES*

CYCLE 31th / 2015

**Extracellular Vesicles Mediate Mesenchymal Stromal
Cell-dependent Regulation of B Cell Functions**




S.S.D. MED/15

Coordinator: Prof. Giovanni Targher

Tutor: Prof. Mauro Krampera

PhD Student: Annalisa Adamo

This work is licensed under a Creative Commons Attribution-NonCommercial-NoDerivs 3.0 Unported License, Italy.
To read a copy of the licence, visit the web page:
<http://creativecommons.org/licenses/by-nc-nd/3.0/>

-  **Attribution** — You must give appropriate credit, provide a link to the license, and indicate if changes were made. You may do so in any reasonable manner, but not in any way that suggests the licensor endorses you or your use.
-  **NonCommercial** — You may not use the material for commercial purposes.
-  **NoDerivatives** — If you remix, transform, or build upon the material, you may not distribute the modified material.

Extracellular Vesicles Mediate Mesenchymal Stromal Cell-dependent Regulation of B Cell Functions

Annalisa Adamo
PhD thesis
Verona, May 29th 2019

ABSTRACT

Mesenchymal stromal cells (MSCs) are adult, multipotent cells of mesodermal origin representing the progenitors of all stromal tissues. MSCs possess significant and broad immunomodulatory functions affecting both adaptive and innate immune responses once MSCs are primed by the inflammatory microenvironment. Recently, the role of extracellular vesicles (EVs) in mediating the therapeutic effects of MSCs has been recognized. Nevertheless, the molecular mechanisms responsible for the immunomodulatory properties of MSC-derived EVs (MSC-EVs) are still poorly characterized. Therefore, we carried out a molecular characterization of MSC-EV content by high-throughput approaches. We analyzed miRNA and protein expression profile in cellular and vesicular compartments both in normal and inflammatory conditions. We found several proteins and miRNAs involved in immunological processes, such as MOES, LG3BP, PTX3, and S10A6 proteins, miR-155-5p, and miR-497-5p. Different *in silico* approaches were also performed to correlate miRNA and protein expression profile and then to evaluate the putative molecules or pathways involved in immune regulatory properties mediated by MSC-EVs. PI3K-AKT signaling pathway and the regulation of actin cytoskeleton were identified and functionally validated *in vitro* as key mediators of MSC/B cell communication mediated by MSC-EVs. In conclusion, we identified different molecules and pathways responsible for immune regulatory properties mediated by MSC-EVs, thus identifying novel therapeutic targets as safer and more useful alternatives to cell or EV-based therapeutic approaches.

SOMMARIO

Le cellule mesenchimali stromali (MSCs) sono cellule adulte multipotenti di origine mesodermica e rappresentano i progenitori di tutti i tessuti stromali. Le MSCs posseggono significative proprietà immunomodulatorie nei confronti delle cellule dell'immunità innata e adattiva, specialmente quando si trovano in un ambiente infiammatorio. L'effetto terapeutico delle MSCs è in parte mediato dal rilascio di vescicole extracellulari (EVs) ma i meccanismi molecolari alla base delle capacità immunomodulatorie delle EVs secrete dalle MSCs (MSC-EVs) non sono stati ancora caratterizzati. In questo studio abbiamo effettuato una caratterizzazione molecolare del contenuto delle MSC-EVs tramite approcci *high-throughput*. In particolare, abbiamo analizzato il profilo di espressione di miRNAs e proteine nel compartimento vescicolare e cellulare in condizioni normali e infiammatorie. I risultati ottenuti mostrano numerose molecole differenzialmente espresse nella condizione infiammatoria rispetto al controllo, le quali includono le proteine MOES, LG3BP, PTX3 e S10A6, e i miRNAs miR-155-5p, and miR-497-5p. Inoltre, abbiamo messo a punto diversi approcci *in silico* per correlare i profili di espressione di miRNAs e proteine al fine di valutare le singole molecole e i pathway coinvolti nell'effetto immunoregolatorio mediato dalle MSC-EVs. Il pathway "PI3K-AKT" e la "regolazione del citoscheletro di actina" sono stati identificati e validati funzionalmente *in vitro* quali mediatori chiave della comunicazione tra MSCs e cellule B mediata dal rilascio di EVs. In conclusione, abbiamo identificato alcune molecole e specifici pathway responsabili delle proprietà immunoregolatorie che caratterizzano le MSC-EVs, i quali potranno rappresentare nel futuro nuovi target terapeutici e un'alternativa più sicura rispetto agli approcci terapeutici basati sull'utilizzo diretto di MSCs o MSC-EVs.

INDEX

1. INTRODUCTION	6
1.1 Extracellular Vesicles	6
1.2 Mesenchymal Stromal Cells and Immunomodulation	7
1.3 Mesenchymal stromal cell-derived extracellular vesicles and immunomodulation	9
1.4 Clinical translation of MSC-EVs: unresolved issues and future perspectives	10
1.4.1 Tumorigenesis and other potential adverse effects of MSC-EVs	10
1.4.2 Large scale MSC-EVs production for clinical use	11
2. AIMS OF THE STUDY	12
3. MATERIALS AND METHODS	13
4. RESULTS	22
5. DISCUSSION AND CONCLUSIONS	32
6. REFERENCES	37
7. FIGURES	48
8. TABLES	64

1. INTRODUCTION

1.1 Extracellular Vesicles

Intercellular communication amongst neighboring cells usually occurs either through cell-to-cell contact or exchange of soluble factors. The latter mechanism rarely occurs through the simple secretion of molecules in the intercellular space, which would lead to their rapid inactivation especially if released at tiny concentrations. A very effective, physiological intercellular communication, even at low molecule concentrations, is represented by the exchange of extracellular vesicles (EVs). EVs consist of a membrane-like envelope, i.e. spherical phospholipid bilayer surrounding various molecules, such as proteins, DNA, different types of RNAs (mRNAs, miRNAs and lncRNAs), lipids and active metabolites. EVs are shedding vesicles acting as molecular shuttles, constantly released by the cells in a sort of assembly chain process, which are characterized by different size and molecular content according to their origin, biogenesis and cellular functional status (1-4). EVs include exosomes (50-100 nm), microvesicles (100-1000 nm), apoptotic bodies (1-5 μm) and some other membrane-bound particles. Exosomes originate from multivesicular body and contain common protein families, such as chaperones (Hsp70 and Hsp90), cytoskeletal proteins (actin, myosin and tubulin), ESCRT proteins (TSG-101 and Alix), proteins involved in transport and fusion (Rab11, Rab7, Rab2 and Annexins) as well as tetraspanin proteins (CD9, CD63, CD81 and CD82) (5-7). Microvesicles result from plasmatic membrane gemmation and contain specific cytoplasmatic proteins of the cells of origin, such as GTP-binding protein, ADP-ribosylation factor 6 (ARF6), matrix metalloproteinases (MMPs), glycoproteins (e.g. GPIb, GPIIb-IIIa), integrins, receptors (e.g. EGFRvIII) and cytoskeletal components (e.g. β -actin and α -actinin-4) (5, 6). In addition, both exosomes and microvesicles contain a large number of molecules, whose functions are still under investigation (8). By contrast, apoptotic bodies are functionally different by the other two kinds of EVs, as they result from the programmed cell death mechanisms and contain DNA, histones and cellular debris derived from cell dismantlement; their formation is a highly controlled mechanism preventing leakage of potentially toxic,

enzymatically active or immunogenic components of dying cells, thereby preventing tissue destruction, inflammation, and autoimmune reactions through cytoskeleton weakening and activation of caspase enzymes. In addition, apoptotic bodies act as a powerful signaling pathway for the microenvironment surrounding dying cells (1-4).

The secretion of EVs is not restricted to mammalian cells, but it has been also identified in lower eukaryotes and prokaryotes, highlighting a high degree of conservation of such communication system and, consequently, its relevance in intercellular communication (9, 10). EVs influence various biological processes directly activating cell surface receptors through protein and bioactive lipid ligands, and delivering effectors including transcription factors, oncogenes, mRNAs, and non-coding regulatory RNAs, such as miRNAs into target cells (11-13).

EVs play a role also during the onset of immune responses. EVs isolated from different cell types possess immunosuppressive effects on T cells and NK cells and play a crucial role in the induction of regulatory T and myeloid cells to further inhibit the immune response (14-16). EVs in co-culture with peripheral blood mononuclear cells (PBMCs) inhibit B cell proliferation and immunoglobulin release (17). Placenta-derived exosomes, purified from the blood of pregnant women, carry immunosuppressive molecules, such as Fas-ligand, which induce tolerance towards the fetus (1-4). On the other hand, EVs may also stimulate the immune system, with the final effect depending on many factors, such as effector and target cells as well as the biological context in which this interaction takes place (1, 4, 18).

1.2 Mesenchymal Stromal Cells and Immunomodulation

Mesenchymal stromal cells (MSCs) are adult, multipotent cells of mesodermal origin representing the progenitors of all stromal tissues. In fact, although they were first identified and isolated from bone marrow (BM), MSCs can be expanded from virtually any tissue with a stromal architecture, including adipose tissue, umbilical cord blood, skin, tendon, muscle, and dental pulp (19-22). The Mesenchymal and Tissue Stem Cell Committee of the International Society

for Cellular Therapy proposed minimal criteria to define human MSCs. First, MSCs must be plastic-adherent when maintained in standard culture conditions. Second, MSC must express CD105, CD73 and CD90, and lack expression of CD45, CD34, CD14 or CD11b, CD79alpha or CD19 and HLA-DR surface molecules. Third, MSCs must differentiate into osteoblasts, adipocytes and chondroblasts *in vitro* (23). Considering their stem properties, the therapeutic potential of MSCs has been increasingly studied in the field of regenerative medicine (24, 25). However, MSCs possess also significant and broad immune modulatory functions affecting both adaptive and innate immune responses once MSCs are primed by the inflammatory microenvironment (26). MSC-mediated immune regulation has been confirmed by both preclinical and clinical studies based on systemic or local MSC administration in a broad spectrum of inflammatory and autoimmune diseases, such as Graft-versus-Host Disease (GvHD) (27), Crohn's disease and enteropathies (28-30), as well as in cardiovascular disease (31, 32), acute kidney injury (33), colitis, sepsis (34), and other disorders (35). MSCs can inhibit natural killer cell (NK) proliferation and activity, T lymphocyte proliferation, dendritic cells (DCs) maturation and B lymphocyte proliferation and activation. Moreover, MSCs may induce regulatory T cell (Treg) expansion (36). The beneficial effect of MSCs was initially ascribed to their ability to home within the inflammation sites, thus stimulating endogenous repair of the injured tissue and modulating immune responses (37-39); actually, only a negligible percentage of systemically administered MSCs is capable of reaching the damaged tissues (40, 41). Therefore, MSC biological activity - in terms of both regeneration and immunomodulation - is supposed to reside in their ability to act at paracrine level through the release of bioactive factors, as observed with cardiomyocytes exposed to hypoxia/reoxygenation (42), or through indirect mechanisms involving phagocytes (43). Several studies identified soluble mediators involved the MSC-immune-modulatory effects, such as interleukins (IL) 6 and 10, prostaglandin E2 (PGE2), hepatocyte growth factor (HGF), indoleamine 2,3-dioxygenase (IDO), nitric oxide (NO), transforming growth factor (TGF)-1 and human leukocyte antigen G (HLA-G) (36).

1.3 Mesenchymal stromal cell-derived extracellular vesicles and Immunomodulation

Recently, the role of EVs in mediating the paracrine effects of MSCs in tissue repair and immunomodulation has been recognized both *in vitro* and *in vivo* (44, 45). Several studies reported an inhibitory activity of MSC-EVs on B, T and NK cell proliferation and activation (45, 46). Moreover, MSC-EVs may polarize monocytes toward M2-like phenotype, which in turn induces CD4⁺ T cell to differentiate into regulatory T cells (47). Blazquez *et al.* also reported the capability of MSC-EVs to inhibit the release of inflammatory cytokines by activated T cells, including IFN- γ (48). In addition, Favaro *et al.* showed that MSC-EVs were able to inhibit IFN- γ production in PBMCs isolated from type 1 diabetic patients, increasing the release of immunomodulatory molecules such as PGE-2, TGF- β , IL-10, and IL-6 and the percentage of regulatory T-cells (49, 50). Furthermore, dendritic cells conditioned with MSC-EVs acquire an immature phenotype with increased IL-10 secretion, thus inducing a reduction of inflammatory T-cell response (49-51).

The therapeutic potential of MSC-EVs in terms of immune regulation has been observed *in vivo* in different disease models. MSC-EV administration reduced Acute Kidney Injury (AKI)-induced oxidative stress, apoptosis and fibrosis (52, 53), and the reduction of pro-inflammatory and an increase of anti-inflammatory cytokines (54, 55). Furthermore, AKI-induced invasion of macrophages and lymphocytes was suppressed following the treatment with MSC-EVs (53, 56, 57). Similar results were observed in acute myocardial infarction (58, 59), liver disease (35, 60, 61), brain and lung injury (62-64).

In a mouse model of acute GvHD, MSC-EVs recapitulated the therapeutic effects of MSCs (65). Systemic infusion of MSC-EVs prolonged the survival and reduced the pathologic damage in multiple GvHD-targeted organs, in association with a suppression of both CD4⁺ and CD8⁺ T cells (65).

1.4 Clinical translation of MSC-EVs: unresolved issues and future perspectives

The use of stem cells for the therapy of human disease, including inflammatory disorders, raised several concerns in the past years leading to challenging objectives to overcome. Such challenges are represented by immune-mediated rejection, senescence-induced genetic instability or loss of function, limited cell survival and malignant transformation (31). In order to produce a sufficient amount of MSCs for clinical application, a considerable *in vitro* expansion is required, leading to potential spontaneous cell transformation (66). Genetic manipulation of MSCs can increase the oncogenic potential of the cells; the transgene may be tumorigenic or cause disruptions in the genome. Furthermore, MSCs are strongly involved in tumor development and various studies reported MSCs as potential source of tumor associated fibroblasts (67). In this light, the choice of translating the therapeutic potential of MSCs to the clinic should be cautiously considered. Experimental studies showed that only a small proportion of MSCs, locally or systematically administered, were incorporated into injured tissues, indicating that the beneficial effects in tissue repair and immunosuppression is mainly mediated by the paracrine activity of MSCs, that includes the release of EVs. This intriguing hypothesis opens novel therapeutic perspectives aimed at developing cell-free strategies based on the use of MSC-EVs.

1.4.1 Tumorigenesis and other potential adverse effects of MSC-EVs

Although EVs clearly lack the potential to directly develop tumors following *in vivo* administration, this does not imply that MSC-EVs administration to human is without any risk of promoting neoplasia. Roccaro *et al.* isolated EVs from BM-MSCs derived from both multiple myeloma patient and healthy controls. In this study, patient-derived MSC-EVs promoted tumor cell growth, whereas healthy donor-derived MSC-EVs inhibited tumor growth both *in vitro* and *in vivo* (68). MSC-EVs are able to modulate the tumor microenvironment, thus creating a niche for cancer cell metastasis and have been found to mimic the effect of MSCs in promoting tumor growth. Zhu *et al.* showed that MSC-EVs co-implanted with

human gastric cancer cells increased tumor growth and angiogenesis (69). However, contradictory results have been reported. Some authors have demonstrated an inhibitory effect towards tumor growth in terms of angiogenesis, drug resistance and cell proliferation (70, 71). The controversial data on the effect of MSC-EVs on tumor growth highlight the complexity of their functions, that could be even opposite depending on several factors, such as the type and the tissue origin of MSCs; in addition, cancer cells may show different responses depending on the tumor model considered. Therefore, it is crucial to carefully evaluate the short- and long- term safety of biologically active EVs for a successful translation of MSC-EVs as a clinical therapy.

1.4.2 Large scale MSC-EVs production for clinical use

Although MSCs are relatively easy to expand using conventional methods, their growth in culture is finite and their biological properties may become altered with repeated passage. To facilitate large-scale MSC-EV production, new batches of MSCs will have to be periodically derived with significant impact on costs of derivation, testing, and validation. MSC immortalization by natural selection or by genetic modification or clonal isolation could be used to overcome this limitation although it would entail safety issues. Chen *et al.* proposed a robust scalable manufacturing process for therapeutic EVs through oncogenic immortalization of human embryonic stem cells (ECS)-derived MSCs (72). In order to enhance purity and yield of MSC-EVs preparation, several approaches have been evaluated, including sequential centrifugation, filtration, and sucrose density gradient to remove contaminating protein aggregates, cell debris and genetic material (73-75). Furthermore, standardized protocols for isolation, quantification and characterization of EVs are still required to clarify their potential clinical applications. Furthermore, because of the capacity of EVs to encapsulate molecules, including proteins and nucleic acids, therapeutic strategies based on engineered EVs are currently on study and the preliminary results are quite promising, thus supporting encouraging prospects for clinical applications.

2. AIMS OF THE STUDY

The beneficial effects possessed by MSCs are reproduced by EVs they release in terms of both regenerative medicine and immunomodulation. The inflammatory environment influences their biological function inducing a higher immunosuppressive activity. Nevertheless, the molecular mechanisms responsible for the immunomodulatory role of MSC-derived EVs are still poorly characterized. This project started from a high-throughput characterization of miRNA and protein expression in MSCs at resting conditions (control MSCs, cMSCs), inflammatory conditions (primed-MSCs, pMSCs) and corresponding EVs (cEVs and pEVs, respectively). Modulated molecules were then functionally validated. In particular, we focused our analysis on those involved in the crosstalk between MSCs and B cells for the following reasons: i. our and other groups have previously demonstrated that B cell activity is strongly modulated by EVs released by MSCs (45, 76); ii. the characterization of the EV-mediated interactions between normal B cells and MSCs represents the basis for studying the same crosstalk in inflammatory and autoimmune diseases as well as in hematological malignancies (77-79). Therefore, the present project was aimed at studying the undisclosed molecular mechanisms regulating the immunosuppressive capability mediated by MSC-EVs. Once these mechanisms are identified, they may represent some novel potential therapeutic targets as safer and more useful alternatives to cell or EV-based therapeutic approaches for inflammatory, autoimmune and proliferative disorders.

3. MATERIALS AND METHODS

Cell cultures

MSCs were isolated from BM aspirates of healthy donors (informed consent, approved by Ethical Committee of Azienda Ospedaliera Universitaria Integrata Verona; N. 1828, May 12, 2010 “Institution of cell and tissue collection for biomedical research in Onco-Hematology”) and characterized as already described (80, 81). Briefly, bone marrow samples from healthy donors were seeded in 5-layer flask at 50.000/cm² nucleated cells density using DMEM supplemented with 10% heat-inactivated fetal bovine serum (FBS), 1% penicillin-streptomycin and 2% L-Glutamine (all from Sigma-Aldrich). After 72 hours, non-adherent cells were removed, and the medium was replaced twice a week. MSCs were detached (0.05% Trypsin-EDTA; Gibco) and harvested when 80% confluent, and then either reseeded at 4.000/cm² cellular density or frozen until use. At the end of P0 (day 12 ± 2), phenotypic analysis of cell surface markers was evaluated by flow cytometry. All experiments were performed between passages 2 and 7. MSCs at 80% confluence were treated or not for 48 hours with 10 ng/mL IFN- γ and 15 ng/mL TNF- α (R&D Systems) to induce inflammatory priming. PBMCs were isolated from human blood using Lymphoprep (Stemcells Technologies). B lymphocytes were isolated from PBMCs using immunomagnetic negative selection (Miltenyi Biotec) with at least 95% cell purity, as evaluated by flow cytometry (80, 81). B lymphocytes were cultured in RPMI medium supplemented with 10% FBS, 1% penicillin-streptomycin and 2% L-Glutamine (all from Sigma-Aldrich). B lymphocytes were activated with 5 μ g/mL anti-human IgM+IgA+IgG (F(ab')₂, Jackson ImmunoResearch), 50 IU/mL rhIL-2 (Novartis), 50 ng/mL polyhistidine-tagged CD40 ligand, 5 μ g/mL anti-polyhistidine antibody (R&D Systems), and 0.5 μ g/mL CpG ODNs (Invitrogen).

Purification, characterization and quantification of MSC-derived EVs

EVs were isolated from conditioned medium by ultracentrifugation as already described (45). Briefly, culture medium (CM) from MSC culture at 80% confluence was aspirated. Cells were washed with phosphate-buffered saline

(PBS) to remove the residual FBS, and fresh culture medium supplemented with 10% EV-depleted FBS, obtained through 18 hour-centrifugation at 100.000 x g was added. After 2 days of incubation, CM from MSCs previously treated or not with inflammatory cytokines was collected and underwent different steps of centrifugation. CM was centrifuged for 10 minutes at 300 x g, 30 minutes at 4 °C at 2000 x g to remove cell debris and apoptotic bodies, and then 90 minutes at 4 °C at 100.000 x g to collect EVs. The pellet was washed with PBS through another step of ultracentrifugation at 100.000 x g for 90 minutes at 4 °C to concentrate and purify EVs. EVs were then resuspended in PBS and stored at - 80 °C. EVs quantification was performed through BCA Protein Assay (Thermo Fisher Scientific). Particle size was evaluated by dynamic light scattering (DLS) measurements using a Zetasizer Nano ZS (Malvern Instruments, 4 mV He-Ne laser, $\lambda_0=633$ nm, $\theta=173^\circ$). To assess the surface marker profile, 10 μ g of EVs were analyzed using MACSPlex Exosome Kit (Miltenyi Biotec), a multiplex bead-based platform that allows the detection of 37 surface epitopes. Samples were analyzed with a FACS Canto II (BD Biosciences). Mean fluorescence values were background corrected according to the protocol.

EV internalization and fluorescence microscopy

To assess EV internalization by B lymphocytes, MSC membranes and RNA were stained with 200 μ M Vybrant Dil Cell-labeling Solution and 500 nM Syto RNA Select (both from Life Technologies), respectively. Then, labelled or unlabeled MSCs were co-cultured in presence of B lymphocytes (1:1) and EV internalization was assessed after 24, 48 and 72 hours. At the end of co-culture, cells were stained with anti-CD45-PerCP-Vio770 (Miltenyi Biotec) and TOPRO-3. EV uptake was analyzed by flow cytometry. Furthermore, EVs were directly stained with 10 μ M Vybrant Dil Cell-labeling Solution and 10 μ M Syto RNA Select and washed with Exosome Spin Column (MW 3000) (Thermo Fisher Scientific). Then, activated B lymphocytes were cultured for 48 hours with 100 μ g of labelled or unlabeled EVs. Cells were loaded into the CytoSpin centrifuge's sample chamber and centrifuged 300xg for 5 minutes. Finally, cells were stained

with 1 µg/mL Hoechst (Thermo Fisher) in PBS and then analyzed by fluorescence microscopy using a Zeiss Axio Observer Z1 microscope (Carl Zeiss).

Sample preparation for shotgun proteomics

EVs were collected and lysed in PBS supplemented with protease inhibitors (Roche) and 1% Sodium Dodecyl Sulphate (SDS) (Bio-Rad). Protein extraction was performed by 5-6 cycles of sonication. Then, ice-cold acetone was added to samples and protein precipitation was conducted overnight at -20°C. Samples were then centrifuged at 14,000xg for 10 min at 4°C, and pellet was resuspended in 100 mM NH₄HCO₃. Protein concentration was measured with BCA Protein Assay. Samples were subjected to denaturation with trifluoroethanol, reduced with DTT 200 mM, alkylation with Iodoacetamide 200 mM, and digested with Trypsin/Lys-C (Promega). The peptide digests were desalted on the Discovery® DSC-18 solid phase extraction (SPE) 96-well Plate. The SPE plate was preconditioned with 1 ml of acetonitrile and 2 ml of water. After the sample loading, the SPE was washed with 1 ml of water. The adsorbed proteins were eluted with 800 µl of acetonitrile:water (80:20). After the desalting, the sample was vacuum-evaporated and reconstituted with 20 µl of 0.05% formic acid in water before LC-MS/MS analysis.

Shotgun Mass Spectrometry

The digested proteins were analyzed with a micro-LC Eksigent Technologies (Eksigent) system interfaced with a 5600+ TripleTOF system (AB Sciex) equipped with DuoSpray Ion Source and Calibrant Delivery System. More detailed information on instrument setting and label-free quantification is available in Supplementary Materials and Methods. Two DDA and three DIA acquisitions were performed (82).

The DDA files were searched using Protein Pilot software v. 4.2 and Mascot v. 2.4. Trypsin/Lys-C as digestion enzyme was specified for both the software. For Mascot we used 2 missed cleavages, the instrument was set to ESI-QUAD-TOF and the following modifications were specified for the search: carbamidomethyl cysteines as fixed modification and oxidized methionine as variable modification.

A search tolerance of 50 ppm was specified for the peptide mass tolerance, and 0.1 Da for the MS/MS tolerance. The charges of the peptides to search for were set to 2+, 3+ and 4+, and the search was set on monoisotopic mass (83, 84).

The UniProt Swiss-Prot reviewed database containing human proteins (version 2015.07.07, containing 42131 sequence entries) was used and a target-decoy database search was performed. False Discovery Rate was fixed at 1%.

The protein quantification was performed by integrating the extracted ion chromatogram of all the unique ions for a given peptide and was carried out with PeakView 2.0 and MarkerView 1.2. Six peptides per protein and six transitions per peptide were extracted from the SWATH files. Shared peptides were excluded as well as peptides with modifications. Peptides with FDR lower than 1.0% were exported in MarkerView for the t-test (85).

Proteomic t-test statistical analysis was performed with MarkerView. Proteins were considered modulated in presence of a fold change ≥ 1.50 or ≤ 0.5 and a p-value < 0.05 .

Western Blot Analysis

Immunoblot analysis on EV candidate proteins was performed as previously described (86). Briefly, protein samples from different biological replicates were diluted 1:1 with Laemmli's sample buffer (62.5 mM Tris-HCl, pH 6.8, 25% glycerol, 2% SDS, 0.01% Bromophenol Blue), heated for 5 min at 90°C, and separated by SDS/polyacrylamide gel electrophoresis (PAGE) on 4-20% T acrylamide gels in Tris/glycine/SDS buffer. After separation on SDS-PAGE, proteins were electroblotted on PVDF membrane and subjected to immunodetection. Amido Black staining (Sigma-Aldrich) was used to confirm equal protein loading in different lanes. Membranes were incubated with the different primary antibodies diluted in 1% non-fat dried milk, 0.05% Tween-20 in Tris-buffered saline for 3 hours at room temperature. Blots were then incubated 1 hour at room temperature with the appropriate horseradish peroxidase (HRP)-conjugated secondary antibody (see the Supplementary information, Table S8). Immunocomplexes were visualized by chemiluminescence using the Chemidoc

MP imaging system (Bio-Rad) and the intensity of the chemiluminescence signal was measured by processing the image with Image Lab software (Bio-Rad).

Univariate and multivariate statistical analysis

Proteomic data were analyzed by univariate and multivariate statistical analyses. The univariate approach consisted in selecting proteins modulated at least in 4 samples among 7 processed samples using a cut off with adjusted p values of <0.05 and fold change of >1.5 or <0.0667 . Principal Component Analysis (PCA) was applied to provide a general overview of the correlations existing between the variables and the existence of sample groups (see Supplementary Materials and Methods). PCA is exploited in Ranking-PCA to select the most discriminating variables (i.e. candidate biomarkers) between two groups of samples and sort them according to their decreasing discrimination ability (87-90).

PLS is a multivariate regression method establishing a relationship between one or more dependent variables (Y) and a group of descriptors (X). X and Y variables are modeled simultaneously, to find the latent variables (LVs) in X that will predict the LVs in Y. PLS can be applied for classification purposes by establishing an appropriate Y related to the association of each sample to a class. Since two classes are present in this case (control and primed samples), a binary Y variable is added to each dataset, coded so that -1 is attributed to control samples and $+1$ to primed samples. The regression is then carried out between X-block variables (protein counts) and the Y just established. This application for classification purposes is called PLS-DA (91). Here, Ranking-PCA was used as selection method to provide the list of all candidate biomarkers in decreasing order of discriminant ability of the final model. The list identified in this way was then used for classification, based on PLS-DA (Marengo et al. 2008), to provide a final model able to discriminate the two classes of samples present. The analysis was done considering 1 PC in Ranking-PCA and 1 LV in the final PLS-DA models (for MSCs, only the first 200 proteins selected by Ranking-PCA were included in the PLS-DA model). Both the selection of the significant proteins by Ranking-PCA and the calculation of the performance ability of the PLS-DA models were obtained by leave-one-out (LOO) cross-validation: all the

replications of the same sample (both control and primed replications) were eliminated in turn from the calculation and used to provide an evaluation of the final predictive ability. Since 7 individuals were available, only LOO was applied, and one individual was eliminated at a time. In Ranking-PCA just one PC was used for calculation, due to the small number of degrees of freedom available. The classification performances were evaluated by calculating model accuracy, i.e. the ratio of correctly assigned samples, and the Non-Error-Rate% (NER%), i.e. the average of the accuracies calculated for each class independently.

RNA extraction and quality controls

Total RNA was extracted using miRNeasy Mini Kit (Qiagen) and miRNA enriched fraction was obtained using mirPremier microRNA Isolation Kit (Sigma Aldrich) according to manufacturer's instructions. RNA was quantified with the Qubit RNA Assay kit (Life Technologies). RNA purity and integrity were assessed at the Nanodrop 1000 spectrophotometer (Thermo Fisher Scientific) and by capillary electrophoresis on an Agilent Bioanalyzer (Agilent Technologies), respectively.

Small RNA Sequencing

Small RNA libraries were prepared using the NebNext Small RNA Library Preparation Kit (New England Biolabs) for miRNA and short non-coding RNAs sequencing according to manufacturer's instructions, starting from 200 ng RNA and using 15 PCR cycles. Each library was analyzed with the High Sensitivity DNA chip (Agilent) using Agilent 2100 Bioanalyzer. Pools of 12 libraries were concentrated with AMPure XP magnetic beads (Beckman Coulter) and eluted in 40 µl of nuclease free water. The eluate from each pool was loaded onto a 6% precast gel (Life Technologies), a \approx 146 bp band was cutted, purified with a 5 µL filter with Qiaquick gel extraction kit (Qiagen) and quantified using the Qubit DNA HS (Life Technologies). The miRNAseq libraries were sequenced on a NextSeq500 sequencer (Illumina) using 75bp-reads and producing on average 20470347,38 reads per sample.

Identification of differentially expressed miRNAs

Illumina sequencing was used to generate small RNA reads from 9 biological replicates of primed and control EVs/MSCs. Raw fastq files were analyzed to evaluate their quality using FastQC software (<http://www.bioinformatics.babraham.ac.uk/projects/fastqc>). Adapter trimming was performed using TrimGalore specifying *length* and *max-length* parameters (https://www.bioinformatics.babraham.ac.uk/projects/trim_galore). After this step, only reads with length between 16 and 26 nucleotides remained for further analysis. Clipped reads were aligned using Bowtie2 to the GRCh38 human genome built from ENSEMBL, using the preset of parameters *very-sensitive-local* to obtain high-score matches (92). The summarization of the reads was performed using featureCounts (93), using the GFF annotation file provided by miRBase. Differential expression analysis was conducted through the R/Bioconductor package DESeq2 comparing primed versus control EV/MSC samples, using a 5% FDR cut-off (94).

Real-time qPCR

For miRNA analysis, 10 ng of RNA was retro-transcribed with TaqMan MicroRNA Reverse Transcription Kit (Applied Biosystems). Relative miRNA expression was determined using TaqMan Universal Master Mix II, no UNG and Taqman microRNA assay (Applied Biosystems) and normalized to U6. All reactions were performed in triplicates and run on LightCycler 480 Instrument II (Roche) following manufacturer's instructions. Data obtained from the qPCR were analyzed using the $\Delta\Delta C_t$ method.

GO annotation and pathway enrichment analysis of differentially expressed proteins

GO annotation of significantly altered proteins expressed in pEVs was performed with DAVID v6.8 Functional Annotation Bioinformatics Tools (<https://david.ncifcrf.gov/>). The enrichment analysis for GO cellular component, biological process and molecular function was done by comparing the GO terms of identified proteins against the human proteome. This analysis detected the

significant ($p_{\text{adj}} < 0.05$) over-representation of GO terms in the submitted dataset. In addition, ClueGO v2.3.3, was used for analyzing significantly enriched KEGG pathways ($p_{\text{adj}} < 0.05$) with the human genome as background (95). The nodes in functionally grouped networks were linked based on their kappa score level (0.4) in ClueGO; the GO Tree Levels ranged from levels 3–8.

GO annotation and pathway enrichment analysis of modulated miRNAs and miRNA targets

Functional enrichment of top 10 (based on adjusted p-value) differentially expressed miRNAs in pEVs and pMSCs was performed using DIANA-miRPath v3.0 (96). The enrichment analysis was conducted on KEGG and GO using only experimentally validated miRNA-target interactions provided by DIANA-TarBase v7.0, with *genes union* as merging algorithm. Furthermore, the parameter *conservative stats* were used to have a more stringent statistical test. Only terms with an adjusted p-value < 0.01 were selected.

***In vitro* cell spreading**

Glass coverslips were coated at room temperature for 2 hours with 5 $\mu\text{g}/\text{mL}$ of F(ab')₂. 15×10^4 B lymphocytes, pre-treated for 24 hours with resting and primed EVs, were left to spread at 37°C on coverslips for different time points. Then, cells were fixed with 4% paraformaldehyde in PBS (ChemCruz), permeabilized with 0.5% Triton X-100 (AppliChem) and stained with DAPI and rhodamine phalloidin (both from Life Technologies). Cell spreading was quantified by measuring the mean cell area (μm^2) by using AxioVision 4.8.2 software (Carl Zeiss).

miRNA mimic transient transfection

Activated B cells were seeded at $2 \times 10^5/200 \mu\text{L}$ per well. After 24 hours, cells were transfected with 10 nM of miR-155-5p mimic (5'UAAUUGCUGAUAUCGUGAU AGGGGU) or negative control miRNA (5'GAUGGCAUU CGAUCAGUUCUA) both from Exiqon using INTERFERin (Polyplus-transfection S.A.). After 6 hours, complete RPMI medium

supplemented with stimuli was added to each well. Finally, cells were harvested for the functional analyses after 24, 96 or 120 hours.

PI3K/AKT signaling pathway expression profile

B lymphocytes were cultured for 4 days in presence or absence of EVs (30 μ g EVs/ 2×10^4 cells) or transfected with miRNA Mimics. At the end of culture, cells were harvested and stained with CD45-PerCpVio700 and Viobility 405/520 Fixable Dye (both from Miltenyi Biotec). Then, cells were fixed and permeabilized using Cell Signalling Buffer Set A (Miltenyi Biotec) and stained with Anti-AKT pS473-Vio515, Anti-AKT Pan (PKB)-APC, Anti-GSK3B pS9-PE, Anti-p70 S6 Kinase-FITC, Anti-S6 pS235/pS236-PE and Anti-S6 pS240-APC (all from Miltenyi Biotec) according to manufacturer's instructions. Protein expression was assessed by flow cytometry. Data analysis was performed using FlowJo software (TreeStar). Data were expressed as mean \pm SEM. Statistical analysis was performed by Pism software (GraphPad) using the Wilcoxon test. $P < 0.05$ was considered statistically significant.

Cell Proliferation and Viability Assay

To evaluate the effect of selected miRNAs on B cell proliferation, cells were activated and stained with 5 μ M carboxyfluorescein succinimidyl ester (CFSE, Life Technologies). After 24 hours, cells were transfected with miRNA mimics and negative control. After 4 days, cells were harvested and stained with anti-human CD45-PerCP-Vio700 (Miltenyi Biotec) and TOPRO-3 Iodide (Life Technologies). The effect of selected miRNA on cell viability was assessed by flow cytometry using AnnexinV/7AAD staining. Following 24 hour-stimulation, cells were transfected with miRNA mimics and negative control. After 24 hours, cells were harvested and stained with anti-human CD45-APC (Miltenyi Biotec), Annexin V-FITC (Miltenyi Biotec) and 7AAD (BD Biosciences). Cell viability was evaluated on CD45^{pos} Annexin V^{neg} 7AAD^{neg} cells using FlowJo software (TreeStar). Data were expressed as mean \pm SEM. Statistical analysis was performed by Prism software (GraphPad) using the Wilcoxon test. $P < 0.05$ was considered statistically significant.

4. RESULTS

Size and surface marker characterization of MSC-derived EVs

To characterize MSC-derived EVs, we first analyzed their size using dynamic light scattering (DLS). We identified two separate, equally represented populations of EVs derived from resting MSCs (**Fig 1 A**). The small-sized EVs, ranging from 30 to 100 nm (peak 40.43 ± 15.63 nm, percentage 46.6%), corresponded to exosomes. The large-sized population of EVs, ranging from 100 to 400 nm (peak 207.7 ± 53.95 nm, percentage 53.4%), corresponded to microvesicles. The percentage of exosomes was significantly higher as compared to microvesicles in EVs derived from primed MSCs (75.1% and 24.9%, respectively) (**Fig. 1 B**). Furthermore, we re-analyzed the size of EVs after freezing and thawing the samples. We observed the same DLS profile, demonstrating that EVs maintained their integrity (**Fig. 1, C and D**). To assess the surface marker profile of MSC-derived EVs, we used a multiplex bead-based platform that allows the detection of 37 surface epitopes. Both resting and primed-EVs were positive for the well-established exosome markers CD63, CD81 and CD9 (**Fig. 1 E**). In particular, CD63 intensity was higher compared to CD81 and CD9 expression. As the cells of origin, MSC-derived EVs were positive for CD29, CD44, CD105 and negative for hematopoietic, epithelial, and cancer stem cell markers (**Fig. 1 F**). Moreover, MSC-derived EVs expressed SSEA-4 (**Fig. 1 F**), an early embryonic glycolipid antigen identifying the adult MSC population derived from BM (97). Furthermore, we found a significant expression of CD146 (**Fig. 1 F**), a typical molecule characterizing a specific subpopulation of MSCs with a higher therapeutic potential (98). Western blot analysis confirmed the surface marker profile of EVs, as far as the exosome marker CD63 and the hMSC-associated markers CD44, CD105, and CD146 are concerned (**Fig. 1 G**).

MSC-derived EV internalization by activated B lymphocytes

To evaluate a possible role of MSC-derived EVs in modulating B cell activity, we first assessed the potential of MSCs to transfer membrane fragments and RNA molecules to activated B lymphocytes. To this aim, activated B lymphocytes were

co-cultured with resting or primed MSCs labelled or not at membrane (Vibrant Dil) and RNA (Syto RNA Select) level with fluorescent probes. The transfer of MSC-derived membrane and RNA was observed at different culture times by flow cytometry. At each time points we observed a higher internalization of cEVs compared to pEVs (**Fig. 2 A**). The same trend was observed considering separately the internalization of MSC-derived membranes and RNA molecules, with a more marked effect on RNA transfer (**Fig. 2, B and C**). We detected a double-positive B cell population receiving MSC-derived EVs containing RNA (**Fig. 2 D**). EVs derived from both resting and primed MSCs were internalized by activated B lymphocytes. Initial incorporation was observed after 24 hours of co-culture, followed by an increase until 72 hours. These observations suggest a possible transfer of EVs devoid of RNA molecules or, alternatively, a rapid degradation of MSC-derived RNA molecules by activated B lymphocytes. To confirm EV internalization, we directly co-cultured activated B cells with double-labelled resting or primed EVs and the incorporation was assessed by fluorescence microscopy (**Fig. 2 E**). Overall, our data showed that the uptake of MSC-derived EVs occurs at both resting and primed conditions, thus highlighting a possible involvement of EVs in modulating B cell activity.

Proteomic profiling of MSCs and EVs

To identify proteins potentially involved in immunomodulatory properties mediated by pEVs, MSCs treated or not with inflammatory stimuli and corresponding EVs were analyzed using shotgun MS. A complete list of the identified proteins is shown in Supplementary information, Table S1 (external file). As expected, the number of identified proteins in the cells is higher compared to that identified in the EV compartment (**Supplementary information, Figure S1, A and C**). Nevertheless, the number of modulated proteins is similar among the two compartments (**Supplementary information, Figure S1 B and Table S2**).

To assess the overall variation of the samples following inflammatory stimuli, shotgun MS data were processed by PCA. The score plot of the first two PCs calculated for EVs (**Fig. 3 A**) and MSCs (**Fig. 3 B**) allows the clear separation of

the sample groups, thus indicating that the information about the inflammatory stimuli is present in the protein profile of both EVs and MSCs samples; nevertheless, in the case of EVs, two samples (BM004 and D24) seem quite different as they are far from the others located at the origin of the axes.

We analyzed differentially expressed proteins in pEVs and pMSCs using both univariate and multivariate approaches. By using the univariate analysis, we found 55 and 39 proteins differentially expressed in pEVs and in pMSCs, respectively (Supplementary information, Table S3, external file). Using the multivariate approach, based on Ranking-PCA followed by PLS-DA, we found 181 and 363 proteins differentially expressed in pEVs and in pMSCs, respectively, considering 1 PC in Ranking-PCA and 1 LV in the final PLS-DA models (for MSCs, only the first 200 proteins selected by Ranking-PCA were included in the PLS-DA model).

Fig. 3 C and D report the score plots of the first 2 LVs for EVs and MSCs, respectively. Selected proteins clearly separate resting from primed samples (BM0004 and D24 EVs samples are no more separated from the others as in PCA analysis). The obtained models allowed the perfect classification of all the replications of all the samples (NER% = 100%, accuracy = 100%), both in fitting and in cross-validation for both EVs and MSCs. The list of candidate biomarkers identified by multivariate analysis and the corresponding regression coefficients are provided in Supplementary information, Table S4 (external file). Variables with a positive coefficient correspond to up-regulated proteins, while those characterized by a negative coefficient correspond to down-regulated proteins. The variables can be ordered according to a decreasing discrimination ability on the basis of the decreasing absolute value of the regression coefficient. The multivariate models were compared to PLS-DA models built including the markers identified as statistically significant by classical univariate statistics (**Fig. 3, E and F**) and provided the same classification performances (100% in fitting and cross-validation for all the samples).

For downstream analyses, we selected significantly modulated proteins obtained using both univariate and multivariate approaches: thus, we found 51 (**Fig. 4 A**) and 39 (**Fig. 4 B**) modulated proteins in pEVs and pMSC respectively. Notably, AAAT, CO1A1, CO1A2, COCA1, FINC and ICAM1 were the 6 proteins

modulated both in pMSCs and pEVs showing the same trend (**Fig. 4 C**). Interestingly, among modulated proteins in pEVs, we found a strong down-regulation of different proteins involved in many processes related to the immune response, such as LG3BP (galectin-3-binding protein), PTX3 (pentraxin 3), CCL5 (C-C motif chemokine 5), ENOA (alpha-enolase), MOES (moesin), and S10A6 (Protein S100-A6). To confirm the results obtained through shotgun MS, we selected 4 proteins according to their immunomodulatory potential and we validated their expression through western blotting. As expected, Galectin-3-binding protein (LG3BP) and pentraxin 3 (PTX3) were up-regulated, while moesin (MOES) and Protein S100-A6 (S10A6) were down-regulated in pEVs compared to cEVs (**Fig. 4 D**).

Protein annotation and Pathway Enrichment Analysis on modulated proteins

Differentially expressed proteins of pEVs and pMSCs were annotated on the basis of the GO terms. Considering the pEVs dataset, we found 20 GO terms significantly enriched in the ‘cellular component’ category (**Fig. 5 A**), most of which are related to exosomes and EVs, and 11 and 14 terms enriched in ‘molecular function’ and ‘biological process’ categories, respectively (**Supplementary information, Figure S2, A and C**). As for the enriched GO terms of differentially expressed proteins in pMSCs, we found only 4 GO terms in the ‘cellular component’ (**Fig. 5 B**), of which the most significant was ‘extracellular exosome’, only one term in ‘molecular function’ category and 10 enriched terms in ‘biological process’ category (**Supplementary information, Figure S2, B and D**). As expected, many terms refer to biological processes related to the immune system and response to inflammatory stimuli.

To identify potentially perturbed molecular pathways, pEV-derived modulated proteins were mapped to terms in the KEGG database and categorized into 35 pathways significantly enriched (adjusted p-value < 0.05) (**Fig. 5, C and E**). Notably, the top 10 pathways included the following terms: (i) ‘PI3K-AKT signaling pathway’, an important pathway involved in cell proliferation, survival and growth; (ii) ‘regulation of actin cytoskeleton’; (iii) ‘focal adhesion’; and (iv) ‘leukocyte trans-endothelial migration’. These pathways are crucial during

leukocyte activation, especially during leukocyte migration through activated venular walls. Pathway enrichment analysis was also performed for deregulated proteins of pMSCs and 8 pathways resulted significantly enriched (**Fig. 5, D and F**). Modulated proteins resulting enriched in these four KEGG pathways were mainly down-regulated (**Fig. 5 G**), thus suggesting a possible inhibition of these pathways in immune effector cells, mediated by pEVs.

pEVs induce a down-regulation of PI3K-AKT signaling pathway in activated B lymphocytes

To evaluate the capability of MSC-derived EVs to modulate the PI3K-AKT signaling pathway, activated B lymphocytes were treated with cEVs or pEVs. The expression and phosphorylation profile of different components of PI3K-AKT signaling pathway (PAN AKT, AKT pS473, GSK3b pS9, p70S6K, S6 pS240, S6 pS235pS236) was evaluated by flow cytometry. We observed a strong up-regulation of the pathway during B cell activation, especially considering the phosphorylation of the ribosomal protein S6, one of the main PI3K-AKT downstream effectors (**Fig. 6 A**). As expected, the treatment with pEVs induced a significant down-modulation of the pathway compared to cEVs (**Fig. 6 B**). We observed a significant reduction of S6 pS235pS236 when activated B lymphocytes were cultured with both cEVs and pEVs. However, the treatment with pEVs led to a significantly higher reduction compared to the treatment with cEVs.

MSC-derived EVs inhibit B cell spreading

The second most significant KEGG pathway enriched in EV-modulated proteins was 'regulation of actin cytoskeleton'. Many works revealed that B cells undergo dramatic morphological reorganization following antigen-mediated activation (99-101). In these mechanisms, the activation of actin cytoskeleton seems to play a crucial role, especially during early events on B cell activation (100). To test the possible role of MSC-derived EVs to promote the reorganization of B cell actin cytoskeleton, we evaluated the ability of B lymphocytes, either pre-treated or not with MSC-derived EVs, to spread on coverslips coated with immobilized F(ab')₂

anti-human IgM/IgA/IgG (102). We first verified the specificity of F(ab')₂ anti-human IgM/IgA/IgG to induce cell spreading (**Fig. 7, A and B**). The percentage of cell spreading after one hour of incubation on coated coverslip was 55%. Spreading cells showed elongated and irregular shape with an average area of $129 \pm 59 \mu\text{m}^2$ (**Fig. 7 B**). B lymphocytes pre-treated with pEVs showed a significantly reduced cell spreading, with a cell area average of $111 \pm 61 \mu\text{m}^2$, as compared to the one treated with cEVs, with a cell area average of $86 \pm 41 \mu\text{m}^2$ (**Fig. 7 C**). In addition, the treatment with cEVs lowered the percentage of spreading cells to 47%, while spreading cells were strongly reduced to 27% when B lymphocytes were treated with pEVs (**Fig. 7 D**) We also observed differences in terms of cell shape in the different experimental conditions. While the morphology of spreading B cells treated with cEVs was similar to the one of the control condition, pEVs induced B cells to retain a spherical shape (**Fig. 7 E**). These results confirmed the potential of MSC-derived EVs to modulate the organization of actin cytoskeleton by inhibiting its activation during the processes of B cell spreading. This observation suggests another possible mechanism of action explaining the immunomodulatory properties mediated by MSC-derived EVs, in addition to the modulation of PI3K-AKT signaling pathway.

miRNA expression profile of MSCs and EVs

To determine miRNA expression pattern in MSCs and EVs following the treatment with inflammatory stimuli, we performed next generation miRNA sequencing. To evaluate the overall variation of the samples, miRNA sequencing data were analyzed by PCA (**Fig. 8, A and B**). PCA revealed a clear separation between cMSCs and pMSCc, while cEVs and pEVs were not clearly separated. The same trend was observed using the hierarchical clustering analysis (HCA) among the 9 samples in terms of significantly differentially expressed miRNAs between cMSCs and pMSCs and corresponding EVs (**Fig. 8, C and D**). Cellular samples were completely divided into two branches, corresponding to the treated and the control groups, while cEVs and pEVs were not well separated. These observations highlight that the impact of inflammatory stimuli on miRNA expression is much more evident in MSCs rather than in EVs. Following the

treatment with inflammatory stimuli, we found 15 miRNAs differentially expressed in pEVs (**Fig. 8 E**), of which 4 up- and 11 down-regulated. Some of them are known to be involved in different immunological responses. In the cellular compartment we found 46 miRNAs differentially expressed between cMSCs and pMSCs (**Fig. 8 F**). Three miRNAs resulted modulated with the same trend both in pMSCs and pEVs, i.e. miR-155-5p, miR-199a-5p and miR-222-3p (**Fig. 8 G**).

To assess the functional role of specific miRNAs in MSC-derived EV immunomodulatory properties towards B lymphocytes, we selected miRNAs for RT-qPCR validation by evaluating their experimentally validated targets (**Supplementary information, Table S5**) that were mapped to the terms in the KEGG database. Eventually, miRNA-155-5p, miRNA-199a-5p, and miRNA-497-5p resulted the most promising miRNAs. **Supplementary Table S6** shows the top 20 pathways significantly enriched (adjusted p-value < 0.05) for each miRNA. Notably, these miRNAs can modulate the PI3K-AKT signaling pathway, one of the pathway that we found impaired following the treatment with MSC-derived EVs. To confirm the results of miRNA-Sequencing, the expression of miRNA-155-5p, miRNA-199a-5p, and miRNA-497-5p was validated through RT-qPCR (**Fig. 8 H**).

miR-155-5p reduce B cell viability and PI3K-AKT signaling pathway

Due to its strong up-regulation in pEVs and its potential role in immunomodulation processes, we investigated the effect of miR-155-5p on B cell activity. Although the over-expression of miR-155-5p in activated B lymphocytes did not affect cell proliferation (data not shown), we observed a significant reduction in cell viability (**Fig. 9 A**). Furthermore, considering that many genes belonging to PI3K-AKT signaling pathway are targeted by miR-155-5p, we assessed its contribution on PI3K-AKT pathway activation. As expected, miR-155-5p contributed to reduce PAN AKT expression and ribosomal protein S6 phosphorylations (**Fig. 9 B**).

miRNA targets annotation and Pathway Enrichment Analysis

As the identification of miRNA targets can provide insights into the biological role of differentially expressed miRNA in pEVs and pMSCs, we used miRTarBase, a resource for experimentally validated microRNA-target interactions, to identify the list of experimentally validated miRNA targets (data not shown). To determine their functions, the targets of the top 10 miRNAs modulated in pEVs and pMSCs were annotated on the basis of the GO terms. **Supplementary Figures S3 A and B** show the top 10 GO terms significantly enriched in the ‘cellular component’, considering EVs and MSCs compartments, respectively. Interestingly, the enrichment profile resulted almost equal into the two compartments. A similar trend occurred also considering ‘molecular function’ and ‘biological process’ categories (**Supplementary information, Figure S3 C and D**). These observations suggest that probably miRNAs modulated in pEVs only reflected the state of miRNA expression profile of the cell of origin. Many terms that we found in the three GO categories were related to the transcription activity, such as ‘gene expression’, ‘RNA binding’, ‘transcription factor binding’, and ‘transcription coactivator activity’. Thus, we could expect that the genes targeted by modulated miRNA in pEVs are involved in the regulation of the transcriptional activity of target cells. Concerning the enriched pathways, **Supplementary Figure S3 G** shows the top 10 KEGG pathways that could be affected by modulated miRNA in pEVs. We observed a strong enrichment of pathways related to cancer, highlighting a potential role of MSC-derived EVs in mediating cancer-related processes. Moreover, we found the following terms already identified with enrichment analysis on modulated proteins: (i) ‘focal adhesion’, and (ii) ‘regulation of actin cytoskeleton’. Thus, the modulation of specific proteins together with the modulation of specific miRNA in pEVs could affect the activity of B lymphocytes, especially during leukocyte migration.

Combination of miRNA and proteomic profiles of MSCs and EVs

To verify possible correlations between miRNA and proteomic profiles, the data from miRNA expression profiles and proteomic determinations were merged by using a multivariate approach. To perform this operation, only the individuals in

common with both characterizations were retained; therefore, 4 samples were considered. Only proteins expressed in at least 2 individuals over 4 were considered. Due to the small number of samples involved, only PCA results are presented; however, to show only the correlation structure of the most discriminating variables, PCA was carried out on the first 200 variables selected by ranking-PCA as the most discriminating for both EVs and MSCs. The score plot of the first two PCs calculated for EVs (**Fig. 10 A**) and MSCs (**Fig. 10 B**) allows the clear separation of the groups of samples.

Looking at the loadings for EVs (**Supplementary information, Table S7**), it is possible to verify that Ranking-PCA first includes mainly miRNA signals (and a lower number of proteins), while the last half of the added signals belongs to the proteomic group. Similar considerations can be drawn from the loadings in the case of MSCs (**Supplementary information, Table S7**); however, in this case Ranking-PCA includes almost exclusively miRNA signals in the first 200 variables and just a few proteins, thus indicating that in the case of MSCs the two characterization profiles are more independent from each other. Positive coefficients correspond to variables (miRNAs or proteins) over-expressed in primed samples, while variables with negative coefficients have the opposite behaviour. The loadings show a strong correlation between miRNA profiles and proteomic signals.

miRNAs differentially expressed in pEVs modulate pathways affected by pEV proteins

To verify other correlations between miRNA and proteomic profiles, we employed an *in-silico* approach to evaluate the possible involvement of miRNAs, differentially expressed in pEVs, in regulating some of the top enriched pathways affected by modulated proteins. We correlated miRNA-Seq and shotgun MS results. To this aim, we evaluated the percentage of genes belonging to ‘PI3K-AKT signaling pathway’, ‘regulation of actin cytoskeleton’, ‘focal adhesion’, and ‘leukocyte trans-endothelial migration’ KEGG pathways targeted by miRNAs differentially expressed in pEVs. All 15 differentially expressed miRNAs targeted more than 50% of genes that constitute ‘PI3K-AKT signaling pathway’ and

'regulation of actin cytoskeleton' pathways (61.8% and 52.8%, respectively) (**Fig. 10, C and D**). Moreover, 14 miRNAs targeted 58% and 72.4% of genes belonging to 'leukocyte trans-endothelial migration' and 'focal adhesion' pathways, respectively (**Fig. 10, E and F**).

5. DISCUSSION AND CONCLUSIONS

EV-mediated cellular communication has become a hot research topic because of increasing evidence of EV involvement in many physiological and pathological conditions. Depending on their molecular composition, EVs can influence several biological processes by directly activating cell surface receptors and delivering molecular effectors into target cells (11-13). The molecular composition of EVs is strictly influenced by the cell of origin and different environmental conditions; accordingly, EVs secreted by different cell types can modulate the immune system depending on such molecular composition (1, 4, 18, 44).

The predominance of paracrine mechanisms in MSC-mediated immunomodulatory effect has been broadly demonstrated (103-106). These mechanisms include the release of EVs responsible for the reduction of immune effector cell activation, especially as far as B and NK cells are considered (45). MSC priming with inflammatory cytokines dramatically enhances their immunosuppressive properties, thus increasing the capability of EVs they release to reduce the immune responses (45). Many studies have confirmed the beneficial effect of MSC-derived EVs *in vivo*, paving the way for alternative cell-free therapeutic approaches in the field of inflammatory and autoimmune diseases (107, 108). Nevertheless, the therapeutic application of MSC-derived EVs is still hampered by the lack of standardized and reproducible methods of EV isolation, characterization and quantification and by the difficulty of large-scale production of EVs for therapeutic purposes. In addition, considering their involvement in several physiological and pathological processes, further pre-clinical studies are necessary to exclude possible adverse or simply undesirable effects of MSC-derived EVs. For this reason, a comprehensive analysis of MSC-derived EVs allows to understand the molecular mechanisms underlying their immunomodulatory properties, thus identifying novel therapeutic targets as safer and more useful alternatives to cell or EV-based therapeutic approaches.

On the other hand, the role and prognostic significance of EVs have been documented in a broad range of hematological malignancies, including B-cell leukemia and lymphoma, with a clear involvement in the development and

progression of the disease (77-79). In all these pathological conditions, BM stromal cells represent a pivotal player in the survival, proliferation, differentiation and chemoresistance of neoplastic B cells (109, 110).

Consequently, in this work we focused the analysis on the crosstalk between MSCs and B cells, as we have recently shown that pMSC-derived EVs strongly modulate B cell activity. Here, we showed the effect of inflammatory stimuli on MSC-derived EV secretion and content in terms of miRNA and protein expression profile. We also correlated EVs content with their immunomodulatory properties towards B lymphocytes.

Notably, inflammatory priming induced MSCs to release a higher percentage of exosomes compared to microvesicles, suggesting that the role of smaller vesicles could be functionally more crucial in mediating MSC-related immunosuppressive mechanisms. As shown by flow cytometry, the internalization of cEVs by B lymphocytes resulted higher than pEVs, probably due to the different size of EVs released by MSCs in normal or inflammatory conditions. Inflammatory stimuli affected not only MSC-derived EV size, but also their protein and miRNA content. Protein expression profile of MSCs and MSC-derived EVs was deeply affected by inflammatory priming. Interestingly, modulated proteins in cellular compartment were mostly involved in the release of extracellular exosomes, thus highlighting the significance of EV release by MSCs during inflammatory processes and, consequently, their role in MSC-mediated immune regulation. Furthermore, modulated proteins in pEVs are involved in different processes related to immunological events, especially during leukocyte activation and migration. Such processes include ‘PI3K-AKT signaling pathway’ and ‘regulation of actin cytoskeleton’. PI3K-AKT signaling pathway is an intracellular pathway affecting the function of several biological processes, such as cell survival, cell cycle progression, and cellular growth (111), while the regulation of actin cytoskeleton is pivotal during leukocyte activation, especially during the early stage of B cell receptor activation (99). The proteins belonging to these pathways resulted down-modulated, thus suggesting their possible involvement during the process of immunosuppression towards effector cells. As expected, pEVs induced a strong down-modulation of PI3K-AKT components and a substantial

impairment of actin reorganization in B lymphocytes during the early stages of activation. These results confirmed the ability of pEVs to modulate essential processes during the immune response mediated by B lymphocytes and suggest some of the potential mechanisms of action underlying the immunomodulatory properties mediated by MSC-derived EVs. Pathway enrichment analysis for modulated proteins in pMSCs revealed only four terms, including ‘antigen processing and presentation’ pathway as significantly enriched, highlighting the well-known capacity of MSCs to present antigen via major histocompatibility complex (MHC) molecules, which are constitutively expressed and up-regulated on MSCs following inflammatory priming (45, 112). Similarly, only the term ‘identical protein binding’ resulted significantly enriched in the molecular function GO category. Taken together, our results showed that inflammatory stimuli mainly affect the protein content of EVs compared to the originating cells, confirming their crucial role and the predominance of paracrine mechanisms in mediating immunomodulatory functions. Focusing on modulated protein in pEVs, we found several proteins involved in many processes related to immune response, such as LG3BP, PTX3, MOES, and S10A6. Galectins are a family of beta-galactoside-binding proteins implicated in modulating cell-cell and cell-matrix interactions. LG3BP promotes integrin-mediated cell adhesion and influences different processes of immune response, such as NK cell activation and lymphokine-activated killer (LAK) cell cytotoxicity (113). PTX3 is involved in the regulation of innate resistance to pathogens and inflammatory reactions. The expression of this protein is induced by inflammatory cytokines in several mesenchymal and epithelial cell types (114). MOES and S10A6 are also involved in immune response mechanisms, especially regarding the organization of actin cytoskeleton and cell motility (115-117). Considering their function, each of such modulated protein could contribute to immune regulatory activity mediated by MSC-derived EVs. In addition, pEVs showed a strong up-regulation of ITI components. ITI represents a family of structurally related plasma serine protease inhibitors involved in extracellular matrix stabilization (118). Frequent loss of expression of ITIH genes is recurring in multiple human solid tumors, thus promoting tumor metastasis (119). This observation further strengthens the role of

MSC-derived EVs in cancer, with a potential therapeutic action in preventing tumor metastasis.

Inflammatory microenvironment affected not only MSC-derived EVs proteins, but also miRNA expression. In consideration of miRNA stability and involvement in modulating gene expression, their role in cell-to-cell communication mediated by EVs has been increasingly studied in the last years. As for miRNA overall variation following inflammatory priming, enriched GO terms resulted similar in pMSCs and pEVs, showing less remarkable differences between cellular and EV compartment in miRNA composition as compared to proteins composition. Modulated miRNAs influence many processes related to transcription activity; accordingly, pathway enrichment analysis showed a strong enrichment of pathways related to cancer in both dataset. On the other hand, there is a clear evidence that MSCs and MSC-derived EVs can enhance or suppress tumor progression depending on tumor model and stage considered (71, 120, 121). Nevertheless, differentially expressed miRNAs in pEVs are also involved in immunomodulatory processes. Among these, we identified 'focal adhesion' and 'regulation of actin cytoskeleton' KEGG pathways, already found amongst modulated proteins. Thus, the modulation of specific proteins together with the modulation of specific miRNAs in pEVs could affect the activity of immune effector cells, especially during leukocyte migration.

Protein and miRNA molecules contained in MSC-derived EVs following inflammatory priming are strictly connected. They could be transferred into target cells and contribute synergistically to the regulation of immune effector cell activity. Notably, we found that all differentially expressed miRNAs in pEVs influence the most significant enriched pathways resulting from the protein differential expression analysis. Furthermore, many of them have a crucial role in immunological processes in different cellular contexts (122). In particular, miRNA-155-5p is one of the most well characterized miRNA regulating immune response (123-125). Here, we showed that miRNA-155-5p has a direct capability to reduce cell viability in activated B lymphocytes. This effect could be in part mediated by its ability to act as negative regulator of PI3K/AKT signalling

pathway, one of the pathway we proved to be impaired following the treatment with MSC-derived EVs.

In summary, our data show that MSC-derived EVs contain several molecules potentially responsible for their immunomodulatory properties and MSC/B-cell crosstalk; in particular, specific molecules modulated in pEVs are capable of influencing immune effector cell activity, especially considering B-cell response, thus representing novel potential therapeutic targets that could be further investigated in the field of inflammatory and autoimmune diseases as well as in neoplastic microenvironment of B-cell malignancies.

6. REFERENCES

1. Théry C, Zitvogel L, Amigorena S. Exosomes: composition, biogenesis and function. *Nature Reviews Immunology* (2002) 2(8):569-79. doi: 10.1038/nri855.
2. Cocucci E, Racchetti G, Meldolesi J. Shedding microvesicles: artefacts no more. *Trends in Cell Biology* (2009) 19(2):43-51. doi: 10.1016/j.tcb.2008.11.003.
3. Raposo G, Stoorvogel W. Extracellular vesicles: Exosomes, microvesicles, and friends. *The Journal of Cell Biology* (2013) 200(4):373-83. doi: 10.1083/jcb.201211138.
4. Théry C, Ostrowski M, Segura E. Membrane vesicles as conveyors of immune responses. *Nature Reviews Immunology* (2009) 9(8):581-93. doi: 10.1038/nri2567.
5. Maas SLN, Breakefield XO, Weaver AM. Extracellular Vesicles: Unique Intercellular Delivery Vehicles. *Trends in Cell Biology* (2017) 27:172-88. doi: 10.1016/j.tcb.2016.11.003.
6. van Niel G, D'Angelo G, Raposo G. Shedding light on the cell biology of extracellular vesicles. *Nature Reviews Molecular Cell Biology* (2018) 19(4):213-28. doi: 10.1038/nrm.2017.125.
7. Colombo M, Moita C, van Niel G, Kowal J, Vigneron J, Benaroch P, et al. Analysis of ESCRT functions in exosome biogenesis, composition and secretion highlights the heterogeneity of extracellular vesicles. *Journal of Cell Science* (2013) 126(24):5553-65. doi: 10.1242/jcs.128868.
8. Abels ER, Breakefield XO. Introduction to Extracellular Vesicles: Biogenesis, RNA Cargo Selection, Content, Release, and Uptake. *Cellular and Molecular Neurobiology* (2016) 36(3):301-12. doi: 10.1007/s10571-016-0366-z.
9. Chatterjee SN, Das J. Electron Microscopic Observations on the Excretion of Cell-wall Material by *Vibrio cholerae*. *Journal of General Microbiology* (1967) 49(1):1-11. doi: 10.1099/00221287-49-1-1.
10. Ellis TN, Leiman SA, Kuehn MJ. Naturally produced outer membrane vesicles from *Pseudomonas aeruginosa* elicit a potent innate immune response via combined sensing of both lipopolysaccharide and protein components. *Infection and immunity* (2010) 78(9):3822-31. doi: 10.1128/IAI.00433-10.
11. Ratajczak J, Miekus K, Kucia M, Zhang J, Reca R, Dvorak P, et al. Embryonic stem cell-derived microvesicles reprogram hematopoietic progenitors: Evidence for horizontal transfer of mRNA and protein delivery. *Leukemia* (2006) 20(5):847-56. doi: 10.1038/sj.leu.2404132.
12. Valadi H, Ekström K, Bossios A, Sjöstrand M, Lee JJ, Lötvall JO. Exosome-mediated transfer of mRNAs and microRNAs is a novel mechanism of genetic exchange between cells. *Nature Cell Biology* (2007) 9(6):654-9. doi: 10.1038/ncb1596.
13. Camussi G, Deregibus M-C, Bruno S, Grange C, Fonsato V, Tetta C. Exosome/microvesicle-mediated epigenetic reprogramming of cells. *American journal of cancer research* (2011) 1(1):98-110. doi: 10.1634/stemcells.2005-0235.
14. Whiteside TL. Immune modulation of T-cell and NK (natural killer) cell activities by TEXs (tumour-derived exosomes). *Biochemical Society transactions* (2013) 41(1):245-51. doi: 10.1042/BST20120265.

15. Wieckowski EU, Visus C, Szajnik M, Szczepanski MJSWJ, Whiteside TL. Tumor-Derived Microvesicles Promote Regulatory T Cell Expansion and Induce Apoptosis in Tumor-Reactive Activated CD8+ T Lymphocytes. *Journal of Immunology* (2009) 183(6):247-53. doi: 10.1111/j.1743-6109.2008.01122.x.Endothelial.
16. Dörsam B, Reiners KS, von Strandmann EP. Cancer-derived extracellular vesicles: friend and foe of tumour immunosurveillance. *Philosophical transactions of the Royal Society of London Series B, Biological sciences* (2018) 373(1737). doi: 10.1098/rstb.2016.0481.
17. Burrello J, Monticone S, Gai C, Gomez Y, Kholia S, Camussi G. Stem Cell-Derived Extracellular Vesicles and Immune-Modulation. *Frontiers in Cell and Developmental Biology* (2016) 4(August):1-10. doi: 10.3389/fcell.2016.00083.
18. Robbins PD, Morelli AE. Regulation of immune responses by extracellular vesicles. *Nature reviews Immunology* (2014) 14(3):195-208. doi: 10.1038/nri3622.
19. da Silva Meirelles L, Chagastelles PC, Nardi NB. Mesenchymal stem cells reside in virtually all post-natal organs and tissues. *Journal of Cell Science* (2006) 119(11):2204-13. doi: 10.1242/jcs.02932.
20. Im G, II, Shin Y-W, Lee K-B. Do adipose tissue-derived mesenchymal stem cells have the same osteogenic and chondrogenic potential as bone marrow-derived cells? *Osteoarthritis and Cartilage* (2005) 13(10):845-53. doi: 10.1016/J.JOCA.2005.05.005.
21. Campagnoli C, Roberts IA, Kumar S, Bennett PR, Bellantuono I, Fisk NM. Identification of mesenchymal stem/progenitor cells in human first-trimester fetal blood, liver, and bone marrow. *Blood* (2001) 98(8):2396-402.
22. Nakashima M, Iohara K, Murakami M. Dental pulp stem cells and regeneration. *Endodontic Topics* (2013) 28(1):38-50. doi: 10.1111/etp.12027.
23. Dominici M LBK, Mueller I, Slaper-Cortenbach I, Marini F, Krause D, Deans R, Keating A, Prockop Dj, Horwitz E. Minimal criteria for defining multipotent mesenchymal stromal cells. The International Society for Cellular Therapy position statement. *Cytotherapy* (2006) 8:315-7.
24. Friedenstein AJ, Deriglasova UF, Kulagina NN, Panasuk AF, Rudakowa SF, Luriá EA, et al. Precursors for fibroblasts in different populations of hematopoietic cells as detected by the in vitro colony assay method. *Experimental hematology* (1974) 2(2):83-92.
25. Pittenger MF, Mackay AM, Beck SC, Al E. Multilineage potential of adult human mesenchymal stem cells. *Science* (1999) 284(April):143-7.
26. Krampera M. Mesenchymal stromal cell ‘licensing’: a multistep process. *Leukemia* (2011) 25(9):1408-14. doi: 10.1038/leu.2011.108.
27. Le Blanc K, Frassoni F, Ball L, Locatelli F, Roelofs H, Lewis I, et al. Mesenchymal stem cells for treatment of steroid-resistant, severe, acute graft-versus-host disease: a phase II study. *The Lancet* (2008) 371(9624):1579-86. doi: 10.1016/S0140-6736(08)60690-X.
28. García-Olmo D, García-Arranz M, Herreros D, Pascual I, Peiro C, Rodríguez-Montes JA. A Phase I Clinical Trial of the Treatment of Crohn's Fistula by Adipose Mesenchymal Stem Cell Transplantation. *Diseases of the Colon & Rectum* (2005) 48(7):1416-23. doi: 10.1007/s10350-005-0052-6.

29. Ciccocioppo R, Russo ML, Bernardo ME, Biagi F, Catenacci L, Avanzini MA, et al. Mesenchymal Stromal Cell Infusions as Rescue Therapy for Corticosteroid-Refractory Adult Autoimmune Enteropathy. *Mayo Clinic Proceedings* (2012) 87(9):909-14. doi: 10.1016/j.mayocp.2012.04.014.
30. Ciccocioppo R, Corazza GR. Mesenchymal stem cells for fistulising Crohn's disease. *The Lancet* (2016) 388(10051):1251-2. doi: 10.1016/S0140-6736(16)31209-0.
31. Patel AN, Genovese J. Potential clinical applications of adult human mesenchymal stem cell (Prochymal®) therapy. *Stem Cells and Cloning: Advances and Applications* (2011) 4:61-72. doi: 10.2147/SCCAA.S11991.
32. Toma C, Fisher A, Wang J, Chen X, Grata M, Leeman J, et al. Vascular Endoluminal Delivery of Mesenchymal Stem Cells Using Acoustic Radiation Force. *Tissue Engineering Part A* (2011) 17(9-10):1457-64. doi: 10.1089/ten.tea.2010.0539.
33. Tögel F, Weiss K, Yang Y, Hu Z, Zhang P, Westenfelder C. Vasculotropic, paracrine actions of infused mesenchymal stem cells are important to the recovery from acute kidney injury. *American Journal of Physiology-Renal Physiology* (2007) 292(5):F1626-F35. doi: 10.1152/ajprenal.00339.2006.
34. Gonzalez-Rey E, Anderson P, González MA, Rico L, Büscher D, Delgado M. Human adult stem cells derived from adipose tissue protect against experimental colitis and sepsis. *Gut* (2009) 58(7):929-39. doi: 10.1136/gut.2008.168534.
35. Haga H, Yan IK, Takahashi K, Matsuda A, Patel T. Extracellular vesicles from bone marrow-derived mesenchymal stem cells improve survival from lethal hepatic failure in mice. *Stem Cells Translational Medicine* (2017) 6(4):1262-72. doi: 10.1002/sctm.16-0226.
36. Bruno S, Deregibus MC, Camussi G. The secretome of mesenchymal stromal cells: Role of extracellular vesicles in immunomodulation. *Immunol Lett* (2015) 168(2):154-8. Epub 2015/06/19. doi: 10.1016/j.imlet.2015.06.007. PubMed PMID: 26086886.
37. Li C, Kong Y, Wang H, Wang S, Yu H, Liu X, et al. Homing of bone marrow mesenchymal stem cells mediated by sphingosine 1-phosphate contributes to liver fibrosis. *Journal of Hepatology* (2009) 50(6):1174-83. doi: 10.1016/J.JHEP.2009.01.028.
38. Toma C, Pittenger MF, Cahill KS, Byrne BJ, Kessler PD. Human mesenchymal stem cells differentiate to a cardiomyocyte phenotype in the adult murine heart. *Circulation* (2002) 105(1):93-8.
39. Hofmann NA, Ortner A, Jacamo RO, Reinisch A, Schallmoser K. Oxygen Sensing Mesenchymal Progenitors Promote Neo-Vasculogenesis in a Humanized Mouse Model In Vivo. *PLoS ONE* (2012) 7(9):44468-. doi: 10.1371/journal.pone.0044468.
40. Beitnes JO, Øie E, Shahdadfar A, Karlsen T, Müller RMB, Aakhus S, et al. Intramyocardial Injections of Human Mesenchymal Stem Cells following Acute Myocardial Infarction Modulate Scar Formation and Improve Left Ventricular Function. *Cell Transplantation* (2012) 21(8):1697-709. doi: 10.3727/096368911X627462.
41. Waszak P, Alphonse R, Vadivel A, Ionescu L, Eaton F, Thébaud B. Preconditioning Enhances the Paracrine Effect of Mesenchymal Stem Cells in

Preventing Oxygen-Induced Neonatal Lung Injury in Rats. *Stem Cells and Development* (2012) 21(15):2789-97. doi: 10.1089/scd.2010.0566.

42. Xiang M-x, He A-n, Wang J-a, Gui C. Protective paracrine effect of mesenchymal stem cells on cardiomyocytes. *Journal of Zhejiang University Science B* (2009) 10(8):619-24. doi: 10.1631/jzus.B0920153.

43. Galleu A, Riffo-Vasquez Y, Trento C, Lomas C, Dolcetti L, Cheung TS, et al. Apoptosis in mesenchymal stromal cells induces in vivo recipient-mediated immunomodulation. *Science Translational Medicine* (2017) 9(416):eaam7828-eaam. doi: 10.1126/scitranslmed.aam7828.

44. Rani S, Ryan AE, Griffin MD, Ritter T. Mesenchymal Stem Cell-derived Extracellular Vesicles: Toward Cell-free Therapeutic Applications. *Molecular therapy : the journal of the American Society of Gene Therapy* (2015) 23(5):812-23. doi: 10.1038/mt.2015.44.

45. Di Trapani M, Bassi G, Midolo M, Gatti A, Kamga PT, Cassaro A, et al. Differential and transferable modulatory effects of mesenchymal stromal cell-derived extracellular vesicles on T, B and NK cell functions. *Scientific Reports* (2016) 6(March):1-13. doi: 10.1038/srep24120.

46. Mokarizadeh A, Delirez N, Morshedi A, Mosayebi G, Farshid AA, Mardani K. Microvesicles derived from mesenchymal stem cells: potent organelles for induction of tolerogenic signaling. *Immunol Lett* (2012) 147(1-2):47-54. Epub 2012/06/19. doi: 10.1016/j.imlet.2012.06.001. PubMed PMID: 22705267.

47. Zhang B, Yin Y, Lai RC, Tan SS, Choo AB, Lim SK. Mesenchymal stem cells secrete immunologically active exosomes. *Stem Cells Dev* (2014) 23(11):1233-44. Epub 2013/12/26. doi: 10.1089/scd.2013.0479. PubMed PMID: 24367916.

48. Blazquez R, Sanchez-Margallo FM, de la Rosa O, Dalemans W, Alvarez V, Tarazona R, et al. Immunomodulatory Potential of Human Adipose Mesenchymal Stem Cells Derived Exosomes on in vitro Stimulated T Cells. *Front Immunol* (2014) 5:556. Epub 2014/11/22. doi: 10.3389/fimmu.2014.00556. PubMed PMID: 25414703; PubMed Central PMCID: PMC4220146.

49. Favaro E, Carpanetto A, Caorsi C, Giovarelli M, Angelini C, Cavallo-Perin P, et al. Human mesenchymal stem cells and derived extracellular vesicles induce regulatory dendritic cells in type 1 diabetic patients. *Diabetologia* (2016) 59(2):325-33. Epub 2015/11/26. doi: 10.1007/s00125-015-3808-0. PubMed PMID: 26592240.

50. Favaro E, Carpanetto A, Lamorte S, Fusco A, Caorsi C, Deregibus MC, et al. Human mesenchymal stem cell-derived microvesicles modulate T cell response to islet antigen glutamic acid decarboxylase in patients with type 1 diabetes. *Diabetologia* (2014) 57(8):1664-73. Epub 2014/05/20. doi: 10.1007/s00125-014-3262-4. PubMed PMID: 24838680.

51. Di Nicola M, Carlo-Stella C, Magni M, Milanese M, Longoni PD, Matteucci P, et al. Human bone marrow stromal cells suppress T-lymphocyte proliferation induced by cellular or nonspecific mitogenic stimuli. *Blood* (2002) 99(10):3838-43. Epub 2002/05/03. PubMed PMID: 11986244.

52. Bruno S, Grange C, Deregibus MC, Calogero RA, Saviozzi S, Collino F, et al. Mesenchymal stem cell-derived microvesicles protect against acute tubular injury. *J Am Soc Nephrol* (2009) 20(5):1053-67. Epub 2009/04/25. doi:

10.1681/ASN.2008070798. PubMed PMID: 19389847; PubMed Central PMCID: PMCPMC2676194.

53. He J, Wang Y, Sun S, Yu M, Wang C, Pei X, et al. Bone marrow stem cells-derived microvesicles protect against renal injury in the mouse remnant kidney model. *Nephrology (Carlton)* (2012) 17(5):493-500. Epub 2012/03/01. doi: 10.1111/j.1440-1797.2012.01589.x. PubMed PMID: 22369283.

54. Lin KC, Yip HK, Shao PL, Wu SC, Chen KH, Chen YT, et al. Combination of adipose-derived mesenchymal stem cells (ADMSC) and ADMSC-derived exosomes for protecting kidney from acute ischemia-reperfusion injury. *Int J Cardiol* (2016) 216:173-85. Epub 2016/05/09. doi: 10.1016/j.ijcard.2016.04.061. PubMed PMID: 27156061.

55. Koch M, Lemke A, Lange C. Extracellular Vesicles from MSC Modulate the Immune Response to Renal Allografts in a MHC Disparate Rat Model. *Stem Cells Int* (2015) 2015:486141. Epub 2015/09/10. doi: 10.1155/2015/486141. PubMed PMID: 26351463; PubMed Central PMCID: PMCPMC4550760.

56. Zou X, Zhang G, Cheng Z, Yin D, Du T, Ju G, et al. Microvesicles derived from human Wharton's Jelly mesenchymal stromal cells ameliorate renal ischemia-reperfusion injury in rats by suppressing CX3CL1. *Stem Cell Res Ther* (2014) 5(2):40. Epub 2014/03/22. doi: 10.1186/scrt428. PubMed PMID: 24646750; PubMed Central PMCID: PMCPMC4055103.

57. Shen B, Liu J, Zhang F, Wang Y, Qin Y, Zhou Z, et al. CCR2 Positive Exosome Released by Mesenchymal Stem Cells Suppresses Macrophage Functions and Alleviates Ischemia/Reperfusion-Induced Renal Injury. *Stem Cells Int* (2016) 2016:1240301. Epub 2016/11/16. doi: 10.1155/2016/1240301. PubMed PMID: 27843457; PubMed Central PMCID: PMCPMC5098097.

58. Shao L, Zhang Y, Lan B, Wang J, Zhang Z, Zhang L, et al. MiRNA-Sequence Indicates That Mesenchymal Stem Cells and Exosomes Have Similar Mechanism to Enhance Cardiac Repair. *BioMed research international* (2017) 2017:4150705-. Epub 2017/01/22. doi: 10.1155/2017/4150705. PubMed PMID: 28203568.

59. Teng X, Chen L, Chen W, Yang J, Yang Z, Shen Z. Mesenchymal Stem Cell-Derived Exosomes Improve the Microenvironment of Infarcted Myocardium Contributing to Angiogenesis and Anti-Inflammation. *Cell Physiol Biochem* (2015) 37(6):2415-24. Epub 2015/12/10. doi: 10.1159/000438594. PubMed PMID: 26646808.

60. Chen L, Xiang B, Wang X, Xiang C. Exosomes derived from human menstrual blood-derived stem cells alleviate fulminant hepatic failure. *Stem Cell Res Ther* (2017) 8(1):9. Epub 2017/01/25. doi: 10.1186/s13287-016-0453-6. PubMed PMID: 28115012; PubMed Central PMCID: PMCPMC5260032.

61. Nong K, Wang W, Niu X, Hu B, Ma C, Bai Y, et al. Hepatoprotective effect of exosomes from human-induced pluripotent stem cell-derived mesenchymal stromal cells against hepatic ischemia-reperfusion injury in rats. *Cytotherapy* (2016) 18(12):1548-59. Epub 2016/11/05. doi: 10.1016/j.jcyt.2016.08.002. PubMed PMID: 27592404.

62. Kim D-k, Nishida H, An SY, Shetty AK, Bartosh TJ, Prockop DJ. Chromatographically isolated CD63+CD81+ extracellular vesicles from mesenchymal stromal cells rescue cognitive impairments after TBI. *Proceedings of the National Academy of Sciences of the United States of America* (2016)

113(1):170-5. Epub 2015/12/22. doi: 10.1073/pnas.1522297113. PubMed PMID: 26699510.

63. Zhang Y, Chopp M, Zhang ZG, Katakowski M, Xin H, Qu C, et al. Systemic administration of cell-free exosomes generated by human bone marrow derived mesenchymal stem cells cultured under 2D and 3D conditions improves functional recovery in rats after traumatic brain injury. *Neurochem Int* (2017) 111:69-81. Epub 2016/08/20. doi: 10.1016/j.neuint.2016.08.003. PubMed PMID: 27539657; PubMed Central PMCID: PMC5311054.

64. Zhu YG, Feng XM, Abbott J, Fang XH, Hao Q, Monsel A, et al. Human mesenchymal stem cell microvesicles for treatment of Escherichia coli endotoxin-induced acute lung injury in mice. *Stem Cells* (2014) 32(1):116-25. Epub 2013/08/14. doi: 10.1002/stem.1504. PubMed PMID: 23939814; PubMed Central PMCID: PMC3947321.

65. Fujii S, Miura Y, Fujishiro A, Shindo T, Shimazu Y, Hirai H, et al. Graft-versus-host disease amelioration by human bone marrow mesenchymal stromal/stem cell-derived extracellular vesicles is associated with peripheral preservation of naive T cell populations. *Stem Cells* (2018) 36(3):434-45.

66. Rubio D, Garcia S, Paz MF, De la Cueva T, Lopez-Fernandez LA, Lloyd AC, et al. Molecular characterization of spontaneous mesenchymal stem cell transformation. *PLoS One* (2008) 3(1):e1398. Epub 2008/01/03. doi: 10.1371/journal.pone.0001398. PubMed PMID: 18167557; PubMed Central PMCID: PMC2151133.

67. Kidd S, Spaeth E, Watson K, Burks J, Lu H, Klopp A, et al. Origins of the tumor microenvironment: quantitative assessment of adipose-derived and bone marrow-derived stroma. *PloS one* (2012) 7(2):e30563-e. doi: 10.1371/journal.pone.0030563. PubMed PMID: 22363446.

68. Roccaro AM, Sacco A, Maiso P, Azab AK, Tai YT, Reagan M, et al. BM mesenchymal stromal cell-derived exosomes facilitate multiple myeloma progression. *Journal of Clinical Investigation* (2013) 123(4):1542-55. doi: 10.1172/JCI66517.

69. Zhu W, Huang L, Li Y, Zhang X, Gu J, Yan Y, et al. Exosomes derived from human bone marrow mesenchymal stem cells promote tumor growth in vivo. *Cancer Letters* (2012) 315(1):28-37. doi: 10.1016/j.canlet.2011.10.002.

70. Bruno S, Collino F, Iavello A, Camussi G. Effects of mesenchymal stromal cell-derived extracellular vesicles on tumor growth. *Frontiers in Immunology* (2014) 5(AUG):1-5. doi: 10.3389/fimmu.2014.00382.

71. Zhang X, Tu H, Yang Y, Fang L, Wu Q, Li J. Mesenchymal Stem Cell-Derived Extracellular Vesicles: Roles in Tumor Growth, Progression, and Drug Resistance. *Stem Cells International* (2017) 2017:1-12. doi: 10.1155/2017/1758139.

72. Chen TS, Arslan F, Yin Y, Tan SS, Lai RC, Choo ABH, et al. Enabling a robust scalable manufacturing process for therapeutic exosomes through oncogenic immortalization of human ESC-derived MSCs. *Journal of translational medicine* (2011) 9:47-. doi: 10.1186/1479-5876-9-47. PubMed PMID: 21513579.

73. Webber J, Clayton A. How pure are your vesicles? *Journal of extracellular vesicles* (2013) 2:10.3402/jev.v2i0.19861. doi: 10.3402/jev.v2i0.19861. PubMed PMID: 24009896.

74. Hupfeld J, Gorr IH, Schwald C, Beaucamp N, Wiechmann K, Kuentzer K, et al. Modulation of mesenchymal stromal cell characteristics by microcarrier culture in bioreactors. *Biotechnol Bioeng* (2014) 111(11):2290-302. Epub 2014/06/04. doi: 10.1002/bit.25281. PubMed PMID: 24890974.
75. Mitchell JP, Court J, Mason MD, Tabi Z, Clayton A. Increased exosome production from tumour cell cultures using the Integra CELLine Culture System. *Journal of Immunological Methods* (2008) 335(1):98-105. doi: <https://doi.org/10.1016/j.jim.2008.03.001>.
76. Laurenzana I, Lamorte D, Trino S, De Luca L, Ambrosino C, Zoppoli P, et al. Extracellular Vesicles: A New Prospective in Crosstalk between Microenvironment and Stem Cells in Hematological Malignancies. *Stem cells international* (2018) 2018:9863194-. doi: 10.1155/2018/9863194.
77. Boyiadzis M, Whiteside TL. *The emerging roles of tumor-derived exosomes in hematological malignancies.* (2017). p. 1259-68.
78. Caivano A, Laurenzana I, De Luca L, La Rocca F, Simeon V, Trino S, et al. High serum levels of extracellular vesicles expressing malignancy-related markers are released in patients with various types of hematological neoplastic disorders. *Tumor Biology* (2015) 36(12):9739-52. doi: 10.1007/s13277-015-3741-3.
79. Caivano A, Del Vecchio L, Musto P. *Do we need to distinguish exosomes from microvesicles in hematological malignancies?* (2017). p. 2009-10.
80. Di Trapani M, Bassi G, Ricciardi M, Fontana E, Bifari F, Pacelli L, et al. Comparative Study of Immune Regulatory Properties of Stem Cells Derived from Different Tissues. *Stem Cells and Development* (2013) 22(22):2990-3002. doi: 10.1089/scd.2013.0204. PubMed PMID: PMC3840473.
81. Menard C, Pacelli L, Bassi G, Dulong J, Bifari F, Bezier I, et al. Clinical-grade mesenchymal stromal cells produced under various good manufacturing practice processes differ in their immunomodulatory properties: standardization of immune quality controls. *Stem Cells and Development* (2013) 22(12):1789-801. doi: 10.1089/scd.2012.0594. PubMed PMID: PMC3668498.
82. Martinotti S, Patrone M, Manfredi M, Gosetti F, Pedrazzi M, Marengo E, et al. HMGB1 Osteo-Modulatory Action on Osteosarcoma SaOS-2 Cell Line: An Integrated Study From Biochemical and -Omics Approaches. *Journal of Cellular Biochemistry* (2016) 117(11):2559-69. doi: 10.1002/jcb.25549.
83. Cvijetic S, Bortolotto V, Manfredi M, Ranzato E, Marengo E, Salem R, et al. Cell autonomous and noncell-autonomous role of NF- κ B p50 in astrocyte-mediated fate specification of adult neural progenitor cells. *Glia* (2017) 65(1):169-81. doi: 10.1002/glia.23085.
84. Albanese P, Manfredi M, Meneghesso A, Marengo E, Saracco G, Barber J, et al. Dynamic reorganization of photosystem II supercomplexes in response to variations in light intensities. *Biochimica et biophysica acta* (2016) 1857(10):1651-60. doi: 10.1016/j.bbabi.2016.06.011.
85. Ortea I, Rodríguez-Ariza A, Chicano-Gálvez E, Arenas Vacas MS, Jurado Gámez B. Discovery of potential protein biomarkers of lung adenocarcinoma in bronchoalveolar lavage fluid by SWATH MS data-independent acquisition and targeted data extraction. *Journal of proteomics* (2016) 138:106-14. doi: 10.1016/j.jprot.2016.02.010.

86. Brandi J, Cecconi D, Cordani M, Torrens-Mas M, Pacchiana R, Dalla Pozza E, et al. The antioxidant uncoupling protein 2 stimulates hnRNPA2/B1, GLUT1 and PKM2 expression and sensitizes pancreas cancer cells to glycolysis inhibition. (2016). doi: 10.1016/j.freeradbiomed.2016.10.499.
87. Marengo E, Robotti E, Bobba M, Gosetti F. The principle of exhaustiveness versus the principle of parsimony: a new approach for the identification of biomarkers from proteomic spot volume datasets based on principal component analysis. *Analytical and Bioanalytical Chemistry* (2010) 397(1):25-41. doi: 10.1007/s00216-009-3390-8.
88. Polati R, Menini M, Robotti E, Millionsi R, Marengo E, Novelli E, et al. Proteomic changes involved in tenderization of bovine Longissimus dorsi muscle during prolonged ageing. *Food Chemistry* (2012) 135(3):2052-69. doi: 10.1016/j.foodchem.2012.06.093.
89. Robotti E, Demartini M, Gosetti F, Calabrese G, Marengo E. Development of a classification and ranking method for the identification of possible biomarkers in two-dimensional gel-electrophoresis based on principal component analysis and variable selection procedures. *Molecular BioSystems* (2011) 7(3):677-. doi: 10.1039/c0mb00124d.
90. Aspesi A, Pavesi E, Robotti E, Crescitelli R, Boria I, Avondo F, et al. Dissecting the transcriptional phenotype of ribosomal protein deficiency: implications for Diamond-Blackfan Anemia. *Gene* (2014) 545(2):282-9. doi: 10.1016/j.gene.2014.04.077.
91. Marengo E, Robotti E, Bobba M, Milli A, Campostrini N, Righetti SC, et al. Application of partial least squares discriminant analysis and variable selection procedures: a 2D-PAGE proteomic study. *Analytical and Bioanalytical Chemistry* (2008) 390(5):1327-42. doi: 10.1007/s00216-008-1837-y.
92. Langmead B, Salzberg SL. Fast gapped-read alignment with Bowtie 2. *Nature Methods* (2012) 9(4):357-9. doi: 10.1038/nmeth.1923.
93. Liao Y, Smyth GK, Shi W. featureCounts: an efficient general purpose program for assigning sequence reads to genomic features. *Bioinformatics* (2014) 30(7):923-30. doi: 10.1093/bioinformatics/btt656.
94. Love MI, Huber W, Anders S. Moderated estimation of fold change and dispersion for RNA-seq data with DESeq2. *Genome Biology* (2014) 15(12):550-. doi: 10.1186/s13059-014-0550-8.
95. Bindea G, Mlecnik B, Hackl H, Charoentong P, Tosolini M, Kirilovsky A, et al. ClueGO: a Cytoscape plug-in to decipher functionally grouped gene ontology and pathway annotation networks. *Bioinformatics* (2009) 25(8):1091-3. doi: 10.1093/bioinformatics/btp101.
96. Vlachos IS, Zagganas K, Paraskevopoulou MD, Georgakilas G, Karagkouni D, Vergoulis T, et al. DIANA-miRPath v3.0: deciphering microRNA function with experimental support. *Nucleic acids research* (2015) 43(W1):W460-6. doi: 10.1093/nar/gkv403.
97. Gang EJ, Bosnakovski D, Figueiredo CA, Visser JW, Perlingeiro RCR. SSEA-4 identifies mesenchymal stem cells from bone marrow. *Blood* (2007) 109(4):1743-51. doi: 10.1182/blood-2005-11-010504.
98. Wu C-C, Liu F-L, Sytwu H-K, Tsai C-Y, Chang D-M. CD146+ mesenchymal stem cells display greater therapeutic potential than CD146- cells

for treating collagen-induced arthritis in mice. *Stem Cell Research & Therapy* (2016) 7(1):23-. doi: 10.1186/s13287-016-0285-4.

99. Song W, Liu C, Upadhyaya A. The pivotal position of the actin cytoskeleton in the initiation and regulation of B cell receptor activation. *Biochimica et biophysica acta* (2014) 1838(2):569-78. doi: 10.1016/j.bbamem.2013.07.016.

100. Harwood NE, Batista FD. *The cytoskeleton coordinates the early events of B-cell activation.* (2011). p. 1-15.

101. Batista FD, Treanor B, Harwood NE. *Visualizing a role for the actin cytoskeleton in the regulation of B-cell activation.* Wiley/Blackwell (10.1111) (2010). p. 191-204.

102. Machtaler S, Dang-Lawson M, Choi K, Jang C, Naus CC, Matsuuchi L. The gap junction protein Cx43 regulates B-lymphocyte spreading and adhesion. *Journal of Cell Science* (2011) 124(15):2611-21. doi: 10.1242/jcs.089532.

103. Follin B, Juhl M, Cohen S, Perderson AE, Kastrup J, Ekblond A. Increased Paracrine Immunomodulatory Potential of Mesenchymal Stromal Cells in Three-Dimensional Culture. *Tissue engineering Part B, Reviews* (2016) 22(4):322-9. doi: 10.1089/ten.TEB.2015.0532.

104. Özdemir AT, Özgül Özdemir RB, Kırmaz C, Sarıboyacı AE, Ünal Halbutoğlları ZS, Özel C, et al. The paracrine immunomodulatory interactions between the human dental pulp derived mesenchymal stem cells and CD4 T cell subsets. *Cellular Immunology* (2016) 310:108-15. doi: 10.1016/j.cellimm.2016.08.008.

105. Fontaine MJ, Shih H, Schäfer R, Pittenger MF. Unraveling the Mesenchymal Stromal Cells' Paracrine Immunomodulatory Effects. *Transfusion Medicine Reviews* (2016) 30(1):37-43. doi: 10.1016/J.TMRV.2015.11.004.

106. Krampera M, Cosmi L, Angeli R, Pasini A, Liotta F, Andreini A, et al. Role for Interferon- γ in the Immunomodulatory Activity of Human Bone Marrow Mesenchymal Stem Cells. *Stem Cells* (2006) 24(2):386-98. doi: 10.1634/stemcells.2005-0008.

107. Kordelas L, Rebmann V, Ludwig AK, Radtke S, Ruesing J, Doeppner TR, et al. MSC-derived exosomes: a novel tool to treat therapy-refractory graft-versus-host disease. *Leukemia* (2014) 28(4):970-3. doi: 10.1038/leu.2014.41.

108. Kilpinen L, Impola U, Sankkila L, Ritamo I, Aatonen M, Kilpinen S, et al. Extracellular membrane vesicles from umbilical cord blood-derived MSC protect against ischemic acute kidney injury, a feature that is lost after inflammatory conditioning. *Journal of extracellular vesicles* (2013) 2. doi: 10.3402/jev.v2i0.21927.

109. Nwabo Kamdje AH, Bassi G, Pacelli L, Malpeli G, Amati E, Nichele I, et al. Role of stromal cell-mediated Notch signaling in CLL resistance to chemotherapy. *Blood cancer journal* (2012) 2(5):e73-e. doi: 10.1038/bcj.2012.17.

110. Kamdje AHN, Mosna F, Bifari F, Lisi V, Bassi G, Malpeli G, et al. Notch-3 and Notch-4 signaling rescue from apoptosis human B-ALL cells in contact with human bone marrow-derived mesenchymal stromal cells. *Blood* (2011) 118(2):380-9. doi: 10.1182/blood-2010-12-326694.

111. Okkenhaug K. Rules of engagement: Distinct functions for the four class I PI3K catalytic isoforms in immunity. *Annals of the New York Academy of Sciences* (2014) 1280(1):24-6. doi: 10.1111/nyas.12027.

112. Hoogduijn MJ. Are mesenchymal stromal cells immune cells? *Arthritis Research & Therapy* (2015) 17(1):88-. doi: 10.1186/s13075-015-0596-3.
113. Brittoli A, Fallarini S, Zhang H, Pieters RJ, Lombardi G. "In vitro" studies on galectin-3 in human natural killer cells. *Immunology Letters* (2018) 194:4-12. doi: 10.1016/J.IMLET.2017.12.004.
114. Ketter P, Yu J-J, Cap AP, Forsthuber T, Arulanandam B. Pentraxin 3: an immune modulator of infection and useful marker for disease severity assessment in sepsis. *Expert Review of Clinical Immunology* (2016) 12(5):501-7. doi: 10.1586/1744666X.2016.1166957.
115. Nedjadi T, Kitteringham N, Campbell F, Jenkins RE, Park BK, Navarro P, et al. S100A6 binds to annexin 2 in pancreatic cancer cells and promotes pancreatic cancer cell motility. *British Journal of Cancer* (2009) 101(7):1145-54. doi: 10.1038/sj.bjc.6605289.
116. Zawawi KH, Kantarci A, Schulze-Späte U, Fujita T, Batista EL, Amar S, et al. Moesin-induced signaling in response to lipopolysaccharide in macrophages. *Journal of periodontal research* (2010) 45(5):589-601. doi: 10.1111/j.1600-0765.2010.01271.x.
117. Pore D, Gupta N. The ezrin-radixin-moesin family of proteins in the regulation of B-cell immune response. *Critical reviews in immunology* (2015) 35(1):15-31.
118. Bost F, Diarra-Mehrpour M, Martin J-P. Inter-alpha-trypsin inhibitor proteoglycan family. A group of proteins binding and stabilizing the extracellular matrix. *European Journal of Biochemistry* (1998) 252(3):339-46. doi: 10.1046/j.1432-1327.1998.2520339.x.
119. Hamm A, Veeck J, Bektas N, Wild PJ, Hartmann A, Heindrichs U, et al. Frequent expression loss of Inter-alpha-trypsin inhibitor heavy chain (ITIHC) genes in multiple human solid tumors: a systematic expression analysis. *BMC cancer* (2008) 8:25-. doi: 10.1186/1471-2407-8-25.
120. Lindoso RS, Collino F, Vieyra A. Extracellular vesicles as regulators of tumor fate: crosstalk among cancer stem cells, tumor cells and mesenchymal stem cells. *Stem Cell Investigation* (2017) 4(9):75-. doi: 10.21037/sci.2017.08.08.
121. Takam Kanga P, Bassi G, Cassaro A, Midolo M, Di Trapani M, Gatti A, et al. Notch signalling drives bone marrow stromal cell-mediated chemoresistance in acute myeloid leukemia. *Oncotarget* (2016) 7(16):21713-27. doi: 10.18632/oncotarget.7964.
122. Paladini L, Fabris L, Bottai G, Raschioni C, Calin GA, Santarpia L. Targeting microRNAs as key modulators of tumor immune response. *Journal of experimental & clinical cancer research : CR* (2016) 35:103-. doi: 10.1186/s13046-016-0375-2.
123. Liu J, Shi K, Chen M, Xu L, Hong J, Hu B, et al. Elevated miR-155 expression induces immunosuppression via CD39+ regulatory T-cells in sepsis patient. *International Journal of Infectious Diseases* (2015) 40:135-41. doi: 10.1016/J.IJID.2015.09.016.
124. Bitar A, De R, Melgar S, Aung KM, Rahman A, Qadri F, et al. Induction of immunomodulatory miR-146a and miR-155 in small intestinal epithelium of *Vibrio cholerae* infected patients at acute stage of cholera. *PLoS One* (2017) 12(3):e0173817. Epub 2017/03/21. doi: 10.1371/journal.pone.0173817. PubMed PMID: 28319200; PubMed Central PMCID: PMC5358779.

125. Schulte LN, Westermann AJ, Vogel J. Differential activation and functional specialization of miR-146 and miR-155 in innate immune sensing. *Nucleic Acids Res* (2013) 41(1):542-53. Epub 2012/11/13. doi: 10.1093/nar/gks1030. PubMed PMID: 23143100; PubMed Central PMCID: PMC3592429.

7. FIGURES

Fig.1

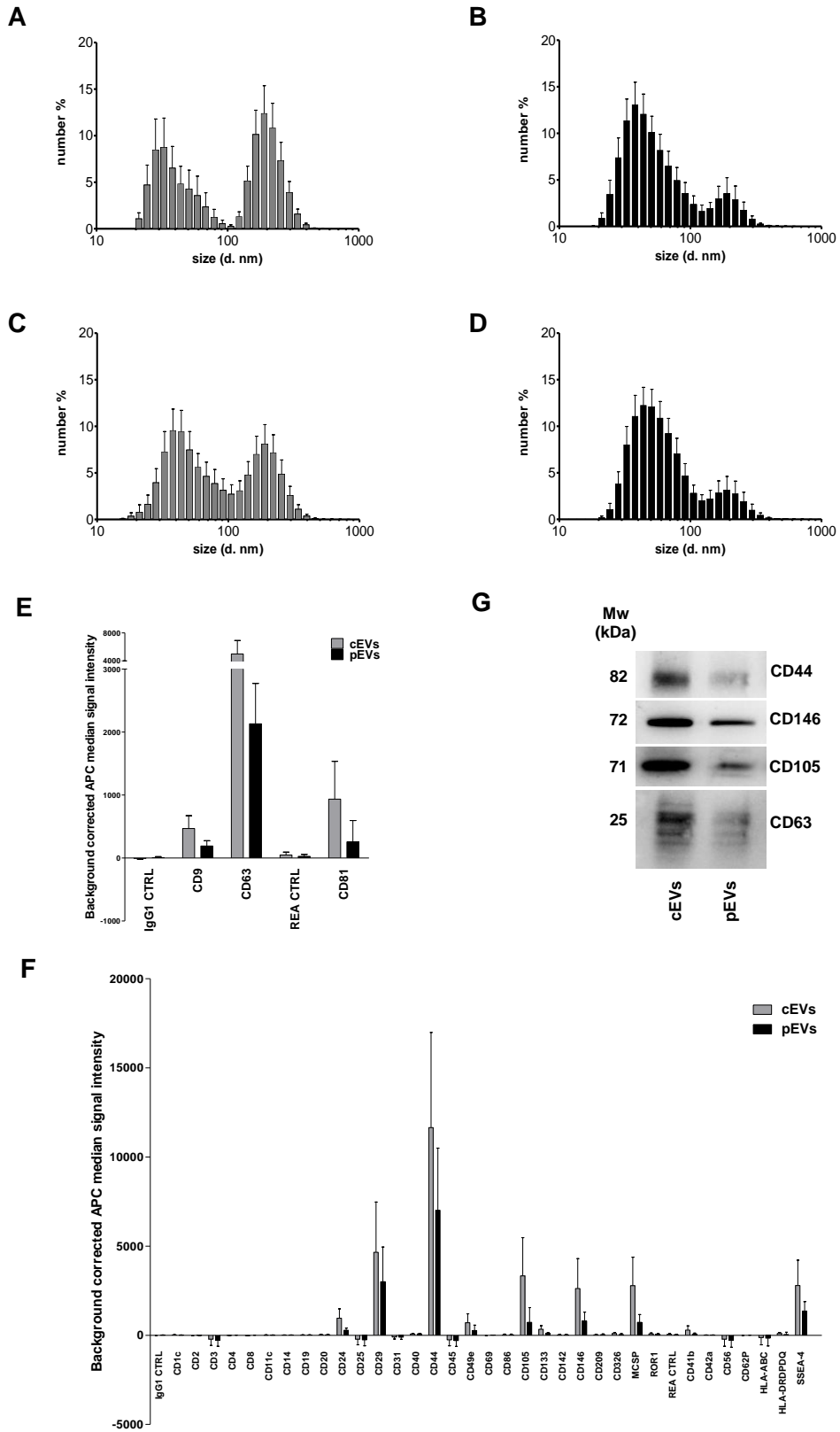


Fig.1 Size and surface marker characterization of MSC-derived EVs. Histograms represent hydrodynamic diameter distribution plots measured on EVs freshly isolated from resting (A) and primed MSC (B) (cEVs exosomes peak 40.43 ± 15.63 nm, percentage 46.6%; cEVs microvesicles peak 207.7 ± 53.95 nm, percentage 53.4%; pEVs exosomes peak 51.17 ± 23.23 nm, percentage 75.1%; pEVs microvesicles peak 200.9 ± 63.57 nm, percentage 24.9%). (C) Hydrodynamic diameter distribution of cEV stored at -80°C (cEVs exosomes peak 51.08 ± 21.07 nm, percentage 59%; cEVs microvesicles peak 196.9 ± 65.34 nm, percentage 41%). (D) Hydrodynamic diameter distribution of pEV stored at -80°C (pEVs exosomes peak 55.91 ± 21.99 nm, percentage 83.6%; pEVs microvesicles peak 201.1 ± 76.45 nm, percentage 16.4%). Error bars represent mean \pm SD obtained from at least five measurements of three independent samples. All experiments were performed in PBS at 25°C . (E) Background corrected median fluorescence intensity of CD9, CD63, CD81 markers and corresponding isotype controls on cEVs and pEVs (n=5). (F) Background corrected median fluorescence intensity of 34 surface epitopes on cEVs and pEVs (n=5). (G) Immunoblot analysis of CD44, CD146, CD105 and CD63 expression in cEVs and pEVs. This blot is representative of three independent experiments showing the same trends.

Fig. 2

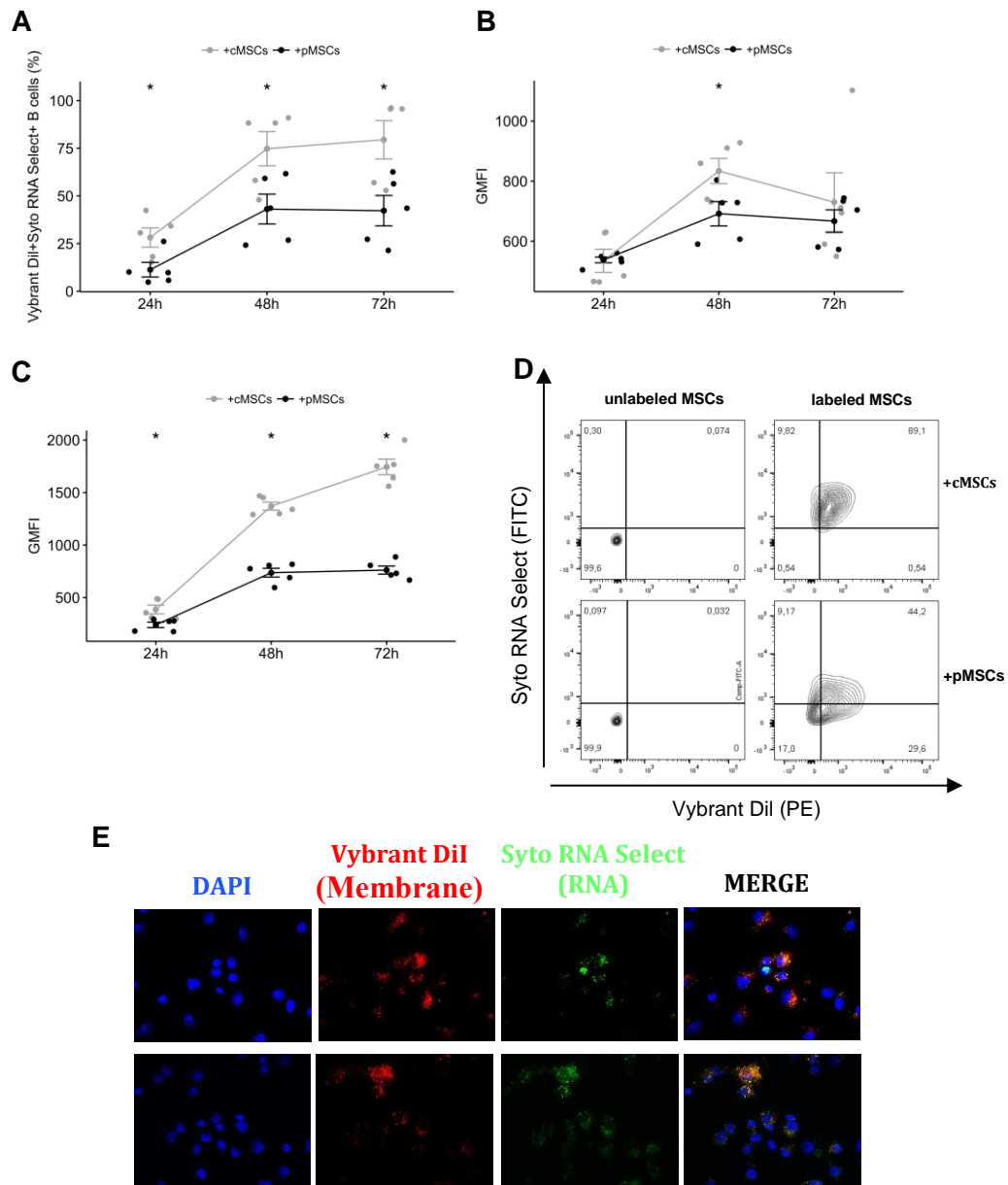


Fig. 2 Incorporation of MSC-EVs and RNA transfer in activated B lymphocytes. (A) Percentage of Vibrant DiI⁺ Syto RNA Select⁺ B cells co-cultured for 24, 48 and 72h with double stained resting or primed MSCs (n=5) *p<0.05. (B) Vybrant DiI (membrane staining) Geometric Mean of Fluorescence Intensity (GMFI) of B cells co-cultured with double stained resting or primed MSCs. (C) Syto RNA Select (RNA staining) GMFI of B cells co-cultured with double stained resting or primed MSCs. (D) Representative FACS analysis of Vibrant DiI⁺ Syto RNA Select⁺ B cells co-cultured for 48h with double stained (right) or not (left) resting or primed MSCs. (E) MSC-EVs were double-stained for

membrane in red (Vybrant DiI) and for RNA in green (Syto RNA Select). Labeled EVs were incubated for 24h on activated B lymphocytes. The four panels show (from the left to the right) B cells stained with DAPI (blue), the internalization of membrane components of cEVs and pEVs (red), the distribution of Syto RNA Select carried by MSC-EVs inside B cells (green), and a merge between the three previous panels (original magnification 400x). The images are representative for three independent experiments with similar results.

Fig. 3

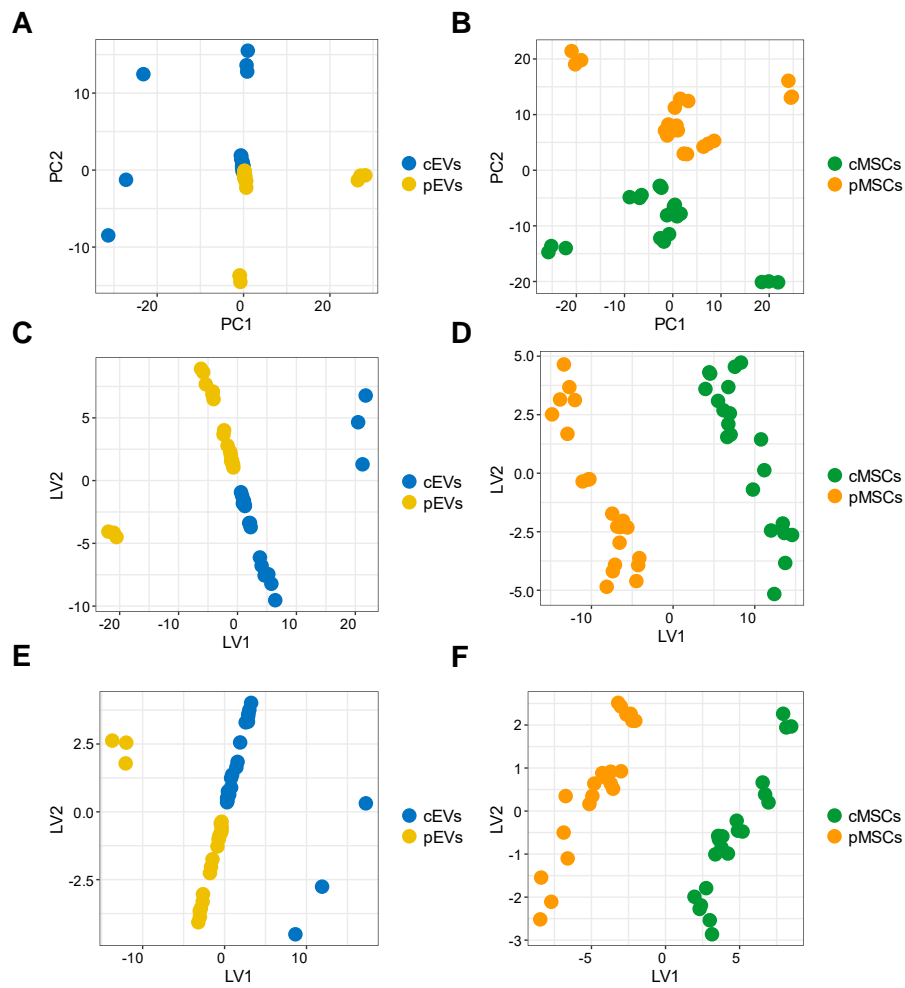


Fig. 3 Overall variation of differentially expresses proteins in MSCs and EVs following inflammatory priming and PLS-DA. Score plot of the first two PCs calculated after the application of PCA to EVs (A) and MSCs (B). Score plot of the first two LVs calculated after the application of PLS-DA to the 181 proteins selected by Ranking-PCA on the EVs dataset (C) and on the first 200 proteins selected by Ranking-PCA on the MSCs dataset (D). Score plot of the first two LVs calculated after the application of PLS-DA to the 55 proteins selected by univariate statistics on the EVs dataset (E) and on the 39 proteins selected by univariate statistics on the MSCs dataset (F).

Fig. 4

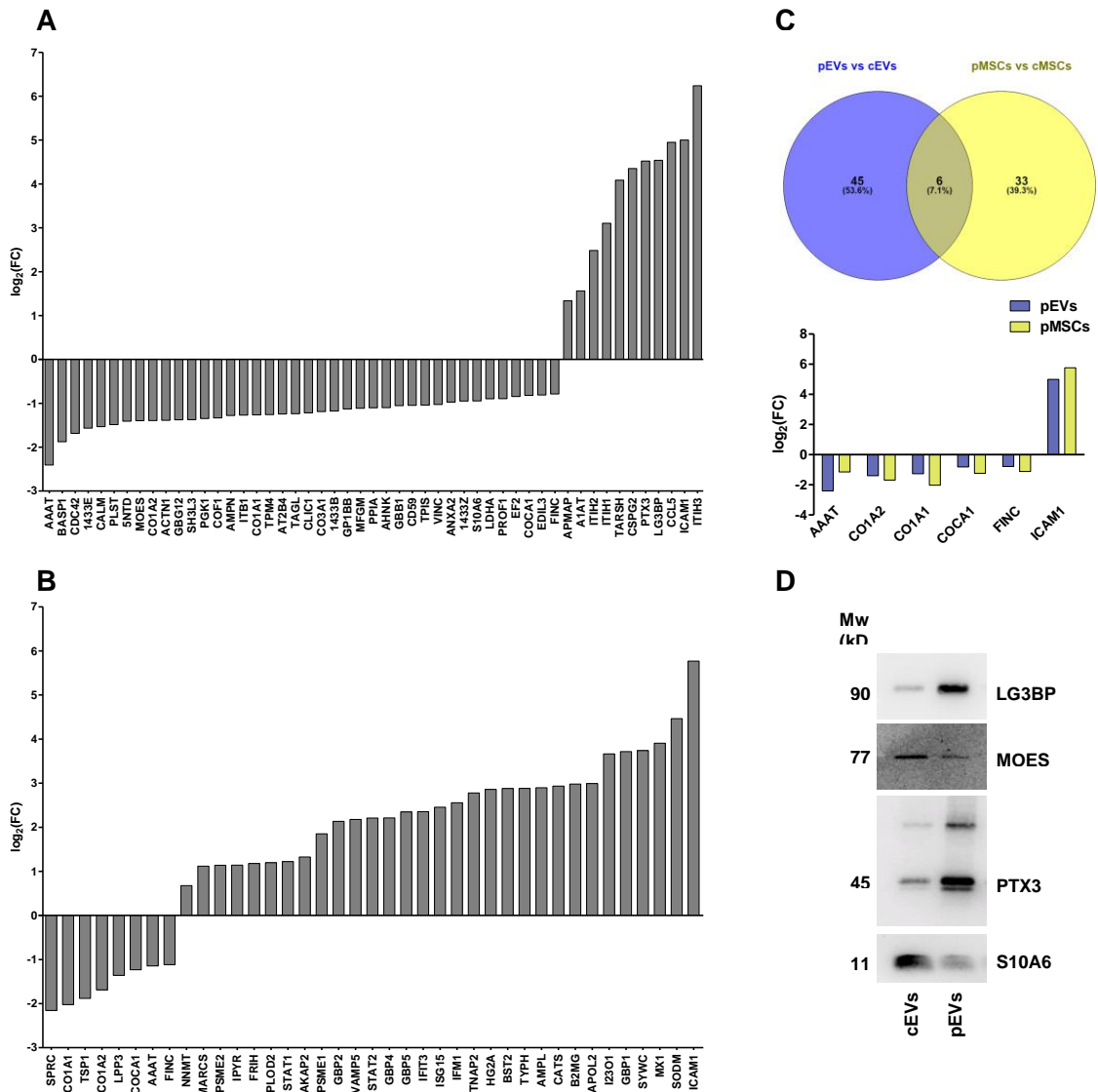


Fig. 5 GO protein annotation and Pathway Enrichment Analysis. Cellular component GO category annotation of differentially expressed proteins in pEVs (A, the top 10 terms are shown) and pMSCs (B). Pathway enrichment analysis on differentially expressed proteins in pEVs (C, the top 10 terms are shown) and pMSCs (D). Terms with adjusted p-value <0.05 were considered significantly enriched. Cytoscape platform based ClueGO/CluePedia pathway analysis and visualization of differentially expressed proteins in pEVs (E) and pMSCs (F). Terms are grouped based on shared genes (kappa score) showed in different colors. The size of nodes indicates the degree of significance. The most significant term defines the name of the group. (G) Modulation of differentially expressed proteins in pEVs enriched in “PI3K-AKT signaling pathway”, “regulation of actin cytoskeleton”, “focal adhesion” and “leukocyte trans-endothelial migration” KEGG pathway ($FC < 0.0667$ or $FC > 1.5$, $p < 0.05$).

Fig. 6

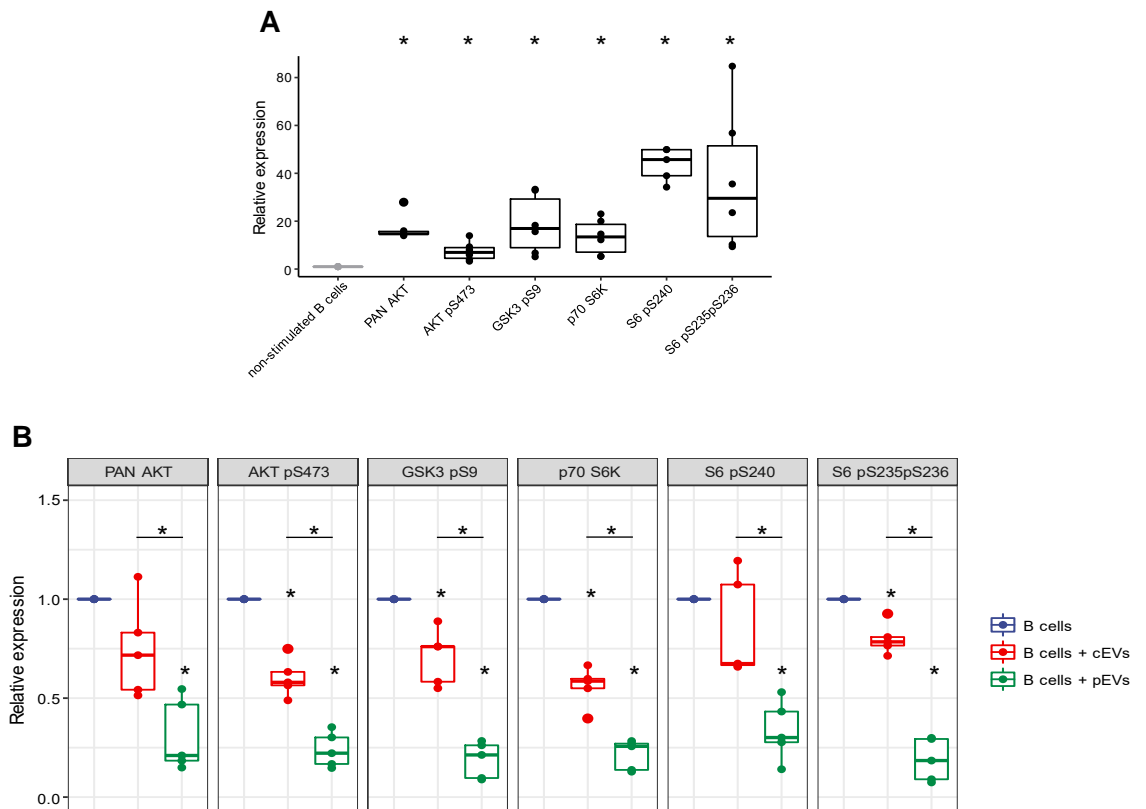


Fig. 6 PI3K-AKT signaling pathway expression in activated B lymphocytes co-cultured with MSC-EVs. (A) Relative expression (fold change) of PAN AKT, AKT pS473, GSK3b pS9, p70S6K, S6 pS240, S6 pS235pS236 in activated B lymphocytes

analyzed by flow cytometry. (B) Relative expression (fold change) of PAN AKT, AKT pS473, GSK3b pS9, p70S6K, S6 pS240, S6 pS235pS236 in activated B lymphocytes treated or not with resting or primed EVs. Wilcoxon test * $p < 0.05$.

Fig. 7

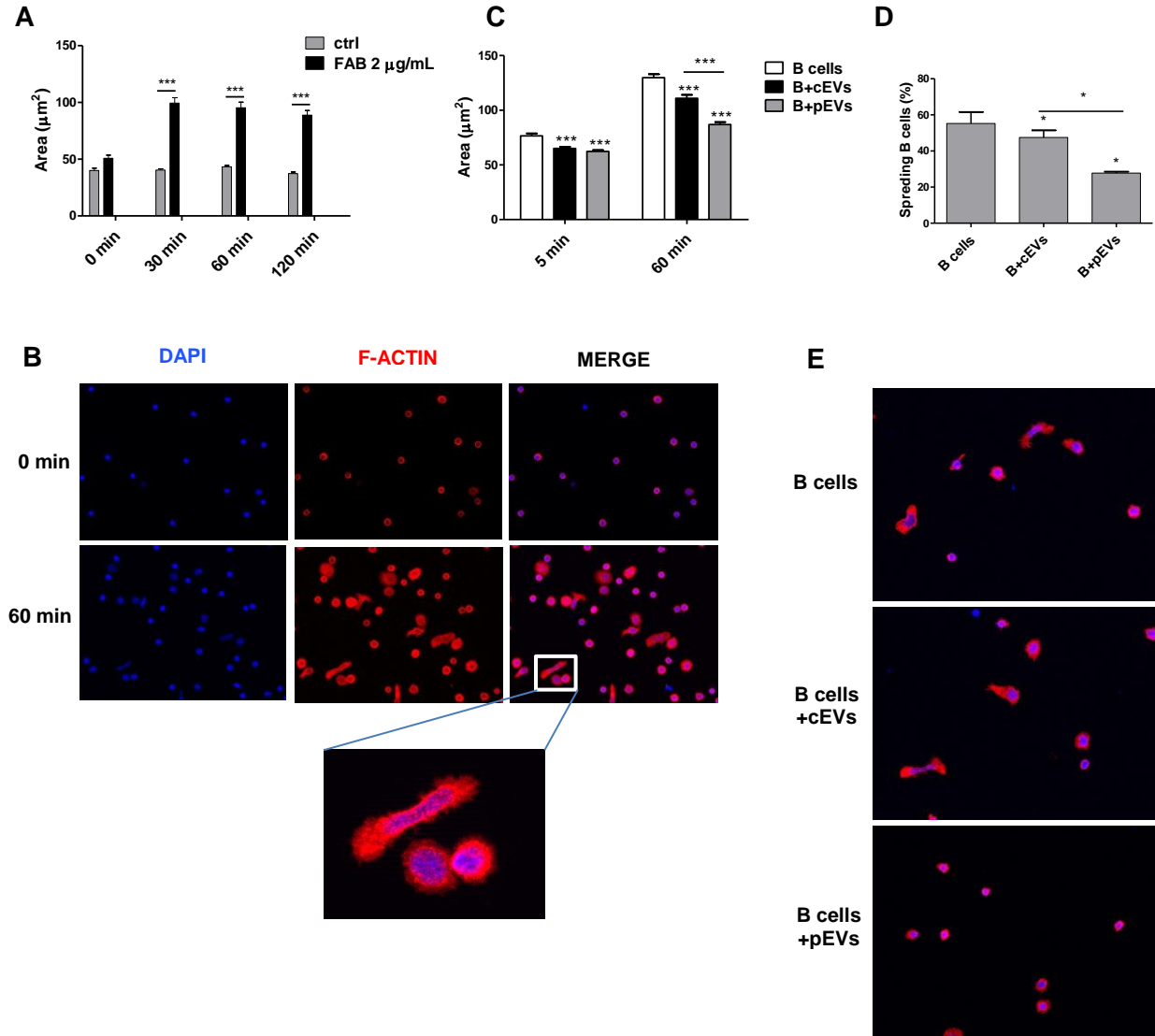
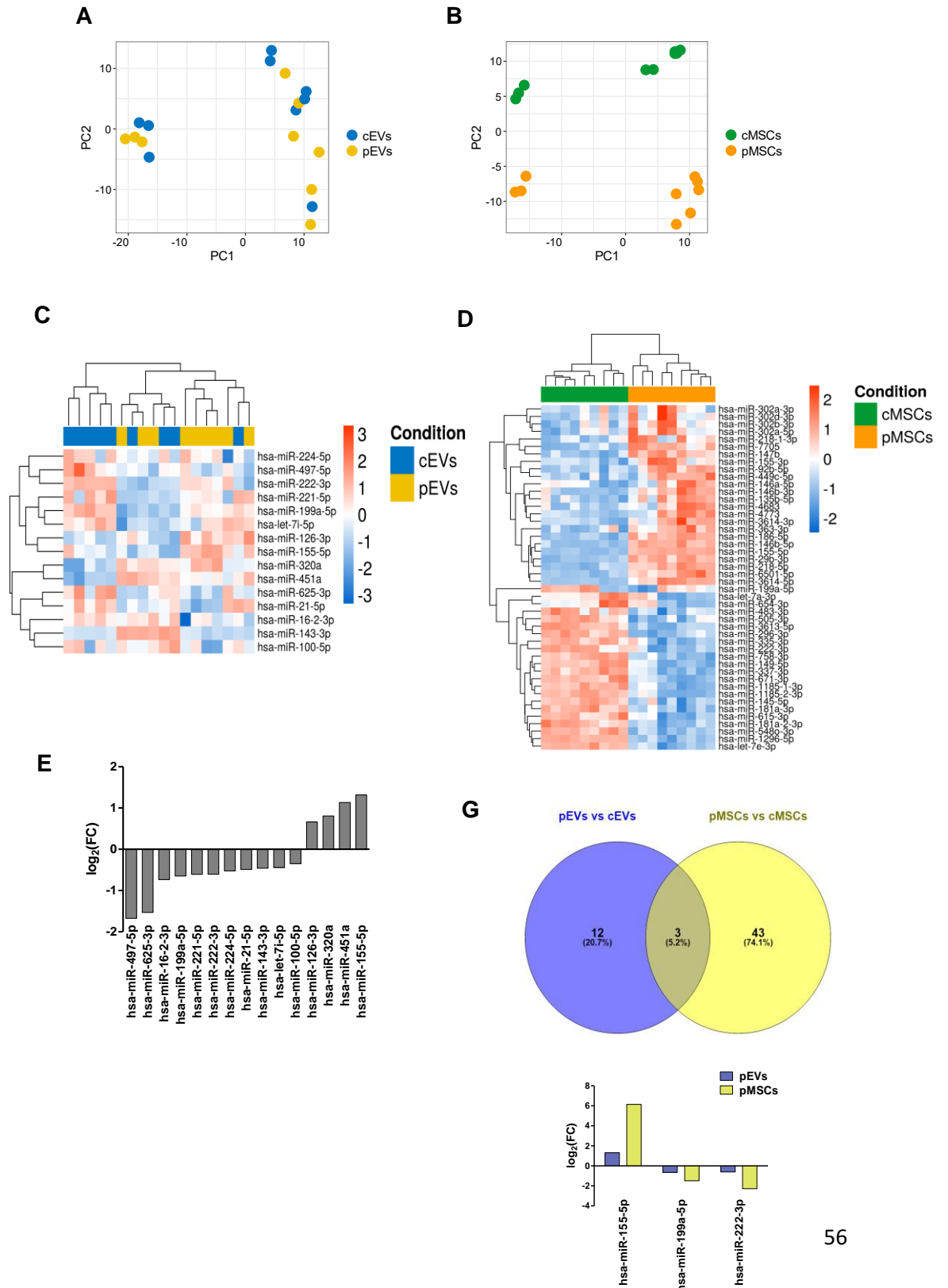


Fig. 7 B cell spreading inhibition mediated by MSC-EVs. (A) Cell area of B cells plated on coverslips coated or not with F(ab')₂ anti-human IgM/IgA/IgG (n=42 to 204). (B) Double-stained B cells with DAPI (blue) and rhodamine phalloidin (F-actin, red) before and after the induction of cell spreading (60 min). (C) Cell area of B cells pre-treated with cEVs or pEVs and then plated on coated coverslips (n=212 to 398). (D) Percentage of spread B cells treated with cEVs or pEVs after 60 min of incubation on coated coverslips. (E) Double-stained B cells with DAPI (blue) and rhodamine phalloidin

(F-actin, red) after 60 min of incubation on coated coverslips. The images are representative for three independent experiments with similar results (Original magnification 400x). Error bars represent mean \pm SEM of three independent experiments. T test * $p < 0.05$, *** $p < 0.001$.

Fig. 8



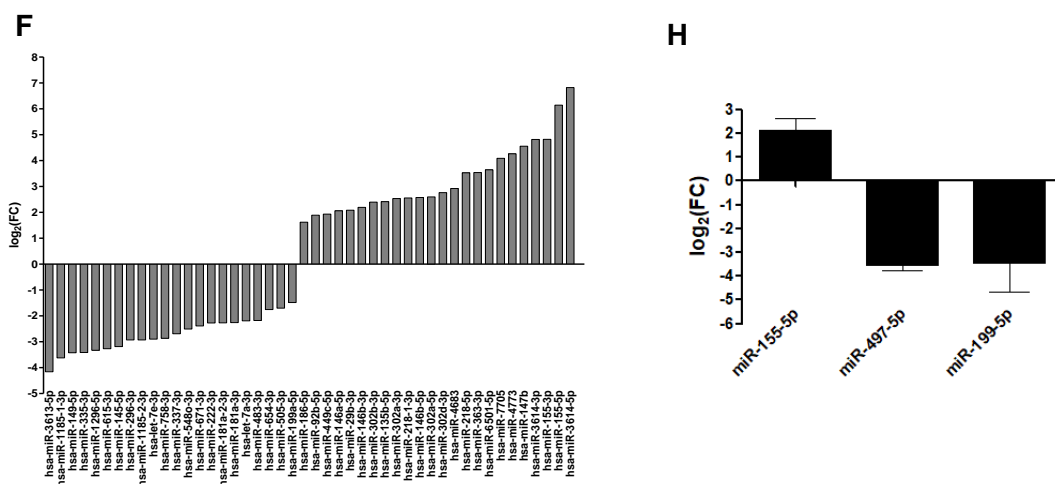


Fig. 8 miRNA expression profile of MSCs and EVs following inflammatory priming. PCA plot calculated using regularized-logarithm transformation of miRNA counts on EVs (A) and MSCs (B) samples. Heatmap summarizing differentially expressed miRNAs in pEVs (C) and pMSCs (D). Bar plot representing the log₂-fold change of differentially expressed miRNAs in pEVs (E) and pMSCs (F). (G) Venn diagram representing common differentially expressed miRNAs in pEVs and pMSCs. (H) RT-qPCR validation of differentially expressed miRNA in pEVs (n≥3). Wilcoxon test *p<0.05.

Fig. 9

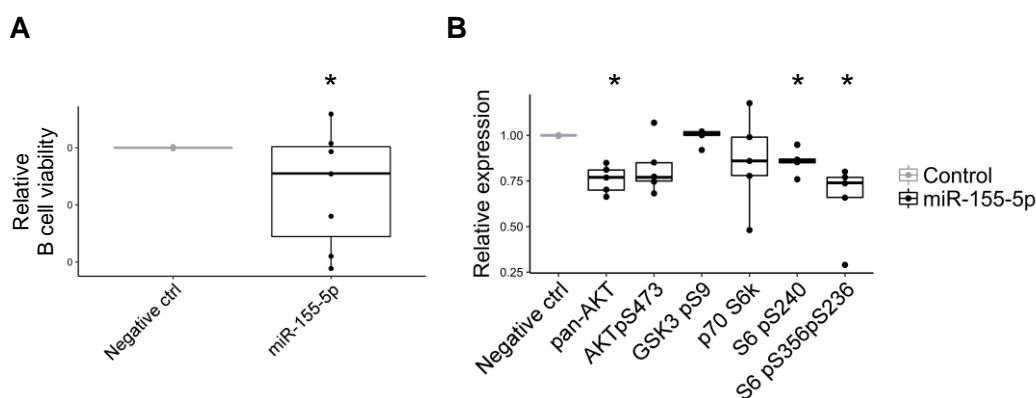
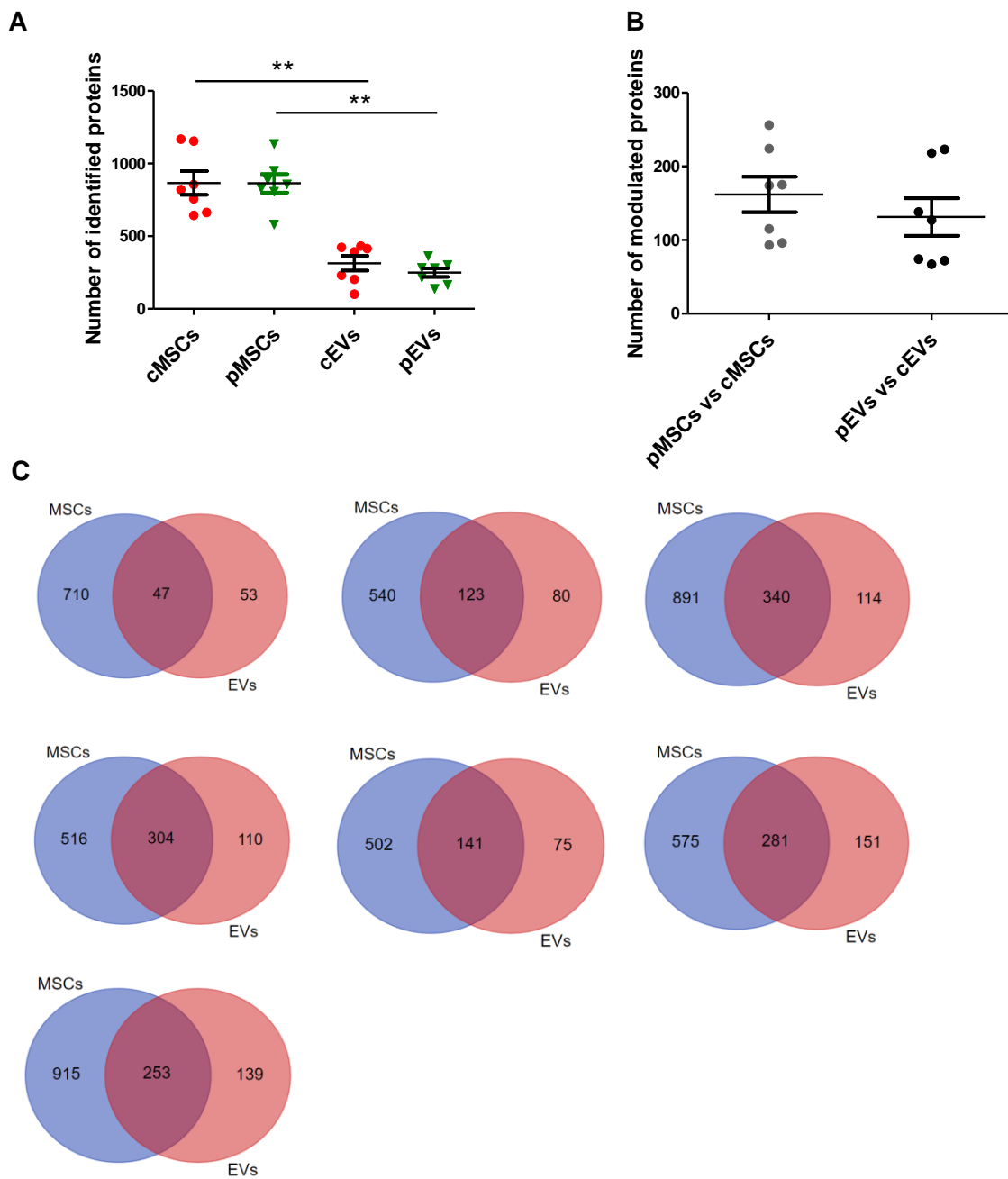
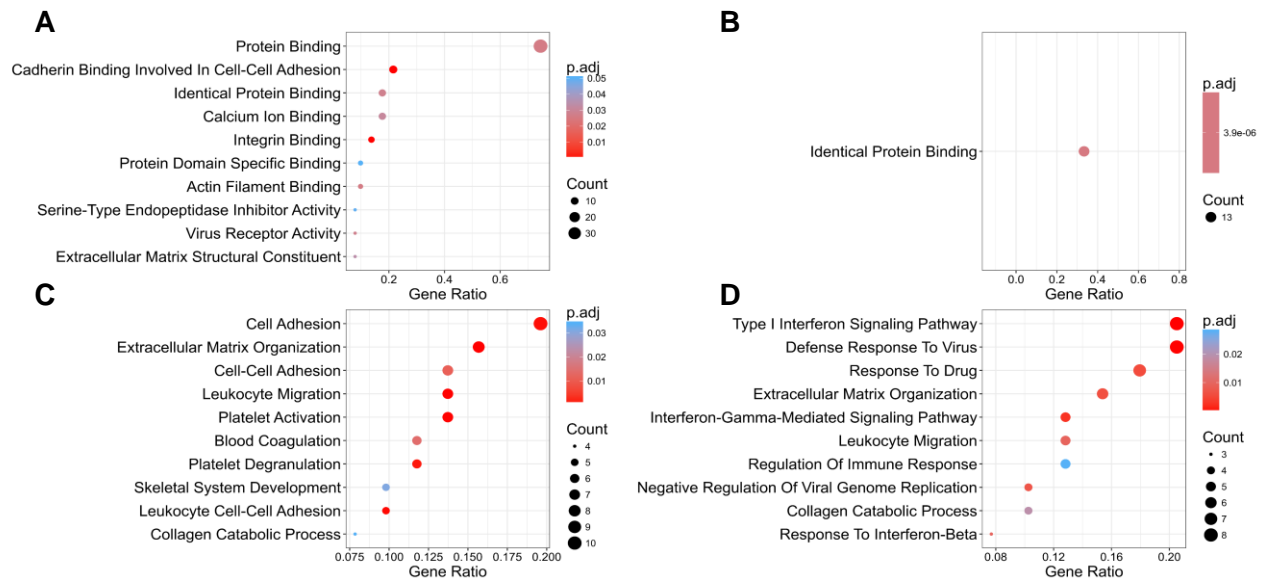


Fig. 9 Effect of miR-155-5p on B cell activity. (A) Relative cell viability of B cells transfected with double-stranded RNA mimic miR-155-5p (n=7). (B) Relative PI3K-AKT signaling pathway expression in B cells transfected with double-stranded RNA mimic miR-155-5p (n=5). Wilcoxon test *p<0.05.

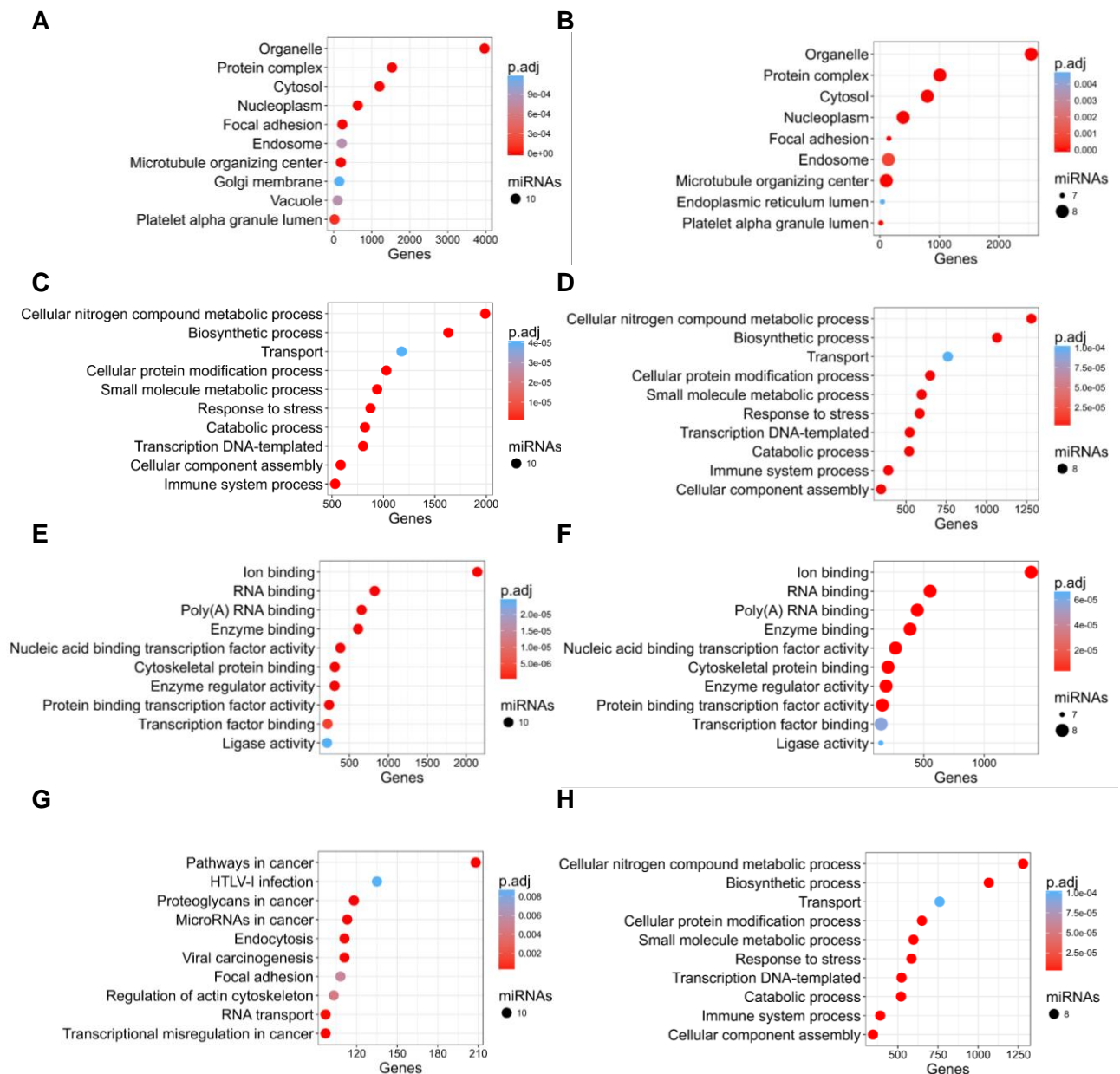


Supplementary information, Figure S1. Identified and modulated proteins in MSCs and EVs. (A) Number of identified proteins in resting and primed MSCs and corresponding vesicles (n=7). (B) Number of modulated proteins in pMSCs and pEVs compared to ctrl. Wilcoxon test $**p < 0.01$. (C) Venn diagrams representing the number of common identified proteins in MSCs and EVs in resting condition for each donor analyzed.



Supplementary information, Figure S2. GO protein annotation.

(A-B) Molecular function GO category annotation of differentially expressed proteins in pEVs (A, the top 10 terms are shown) and pMSCs (B). (C-D) Biological process GO category annotation of differentially expressed proteins in pEVs (C, the top 10 terms are shown) and pMSCs (D). Terms with adjusted p-value < 0.05 were considered significantly enriched.



Supplementary information, Figure S3. Functional enrichment on miRNA targets.

(A-D) Experimentally validated targets of the top 10 miRNAs differentially expressed in pEVs and pMSCs were mapped to terms in the GO database to get enrichment analyses in the “cellular component” (A-B, respectively), “biological process” (C-D, respectively), and “molecular function” (E-F, respectively) categories. (G-H) Pathway enrichment analysis on experimentally validated targets of the top 10 miRNAs differentially expressed in pEVs (G) and pMSCs (H). Terms with adjusted p-value<0.05 were considered significantly enriched. Panels show the top 10 enriched terms.

8. TABLES

Mesenchymal Stromal Cells

	Identified proteins		Modulated proteins (pMSCs vs cMSCs)	
	cMSCs	pMSCs	FC>1.5	FC<0.667
D24	1154	951	69	46
D21	663	857	60	33
D8	757	807	47	49
D29	821	829	64	111
BM004	643	581	54	120
D33	856	1136	179	77
D36	1168	887	70	154

Extracellular Vesicles

	Identified proteins		Modulated proteins (pEVs vs cEVs)	
	cEVs	pEVs	FC>1.5	FC<0.667
D24	423	302	110	113
D21	203	165	18	54
D8	100	138	58	9
D29	414	363	21	53
BM004	230	216	49	78
D33	432	281	46	172
D36	392	282	23	115

Supplementary information, Table S2. Identified and modulated proteins in resting and primed MSCs and corresponding EVs using shotgun MS.

miRNA ID	Experimentally validated miRNA targets
hsa-miR-155-5p	MEIS1, TAB2, MECP2, SOCS1, MSH6, MSH2, MLH1, INPP5D, DET1, SMAD5, HIVEP2, ZNF652, ZIC3, BACH1, JARID2, APC, WDFY1, VAMP3, UBE2J1, TXNRD1, TXNDC12, TRIP13, TRIM32, TRAM1, TNFRSF10A, TBCA, TACSTD2, SYPL1, SYNE2, SNAP29, SMAD1, SLC30A1, SH3BP4, SDCBP, SCAMP1, RHEB, RCOR1, RCN2, RAI14, RAB6A, RAB5C, RAB34, RAB27B, RAB23, PTPRJ, PRKCI, PRAF2, PPP5C, PPL, POLE4, POLE3, PODXL, PLXND1, PKN2, PICALM, PHC2, PDLIM5, PDE3A, NT5E, NARS, MYO1E, MYO10, MSI2, MPZL1, MOSPD2, MARC1, METTL7A, LY6K, LPL, UFL1, HSDL1, HSD17B12, GNA13, FMNL2, FADS1, DSG2, DPP7, DNAJC19, DNAJB1, DHX40, CYP51A1, CUL4B, CTNNA1, CLDN1, CHAF1A, CEBPB, CDK5RAP3, CFBF, BRPF3, BET1, ATP6V1C1, ATG3, ARL5B, ARL10, ARID2, ARFIP2, ARFIP1, ANKFY1, AMIGO2, TM6SF1, MATR3, LDOC1, JADE1, RHOA, AGTR1, TP53INP1, FGF7, IKBKE, NFATC2IP, CUX1, BCAT1, SPI1, CTLA4, EDN1, FOXO3, MAFB, TSHZ3, RUNX2, IFNGR1, ZNF236, LAT2, PAPOLA, EHD1, SERTAD2, PELI1, KBTBD2, HNRNPA3P1, SLC39A10, KRAS, CAMTA1, NAMPT, CREBRF, ETS1, TLE4, FAR1, EDEM3, TWF1, C3orf58, SLC25A40, PSMG1, IKBIP, LCLAT1, VEZF1, SACM1L, DCAF7, ERMP1, KRT80, FLI1, DOCK4, CYR61, ICAM1, SELE, SMAD2, MYB, SKI, WTH3DI, RNF123, CSF1R, SOX6, CKAP5, JUN, PKIA, CSNK1A1, GCSAM, KDM3A, UQCRFS1, IL13RA1, FADD, BCL6, MITF, MAP3K10, NOS3, UBR4, PAXX, MECR, LUC7L2, TCEA1, ANAPC16, C17orf80, SLC27A2, XPC, EIF3G, EIF2B5, UBA3, EIF3E, PCYOX1, EXOC7, QPCTL, DYNC2H1, GLIPR2, DNAAF5, UGT8, HSPB11, CCDC137, GLB1, LRRC40, VBP1, MGST2, GNB4, JUP, DNAJC2, GOLPH3, DRAP1, NOB1, SLC1A5, RAB14, YBX3, SLC39A14, UBE2J2, EIF4A1, CAB39L, MYLK, EIF2B2, CNDP2, RTN3, TMBIM6, EIF4G2, CDC42BPB, MYD88, ADH5, EIF3C, QRICH1, CYFIP1, PSIP1, SIN3A, STK24, AGL, METAP2, SPIN1, FAM98B, ERI1, COLGALT1, UGDH, LNPBK, XPO1, PALLD, MUT, RAP1B, BAG5, LPGAT1, GCFC2, EXOSC2, LNX2, ZNF248, CHD9, MEF2A, CAB39, CLUAP1, CARD11, PCDH9, ZNF561, CARHSP1, C16orf62, LIN7C, CBR4, ECI1, OSBPL10, EIF4E2, TGM2, SLC9A3R2, CHAF1B, PPFIBP1, UBXN1, ESRRB, GAPVD1, MIA2, RBM42, MFF, NEU1, SCD, UBE2D2, OVCA2, EIF3CL, AURKA, P3H3, FUBP1, RETSAT, MPP2, KIAA0368, NES, KIF22, PACSIN2, SLC25A19, IPO8, GPT2, OGFOD1, AKR7A2, TRMT1, MCAM, INA, SNX6, PDAP1, PCNT, FIP1L1, MTAP, CEP55,

	<p>AIFM1, PPM1G, PAM16, PLK1, AURKB, NASP, NUPL2, NCKAP1, EXOC2, SEC24B, RRM2, GRPEL1, ALDH9A1, AP1G1, LUZP1, RPRD1A, NAA25, RP2, NUP155, OTULIN, TMX3, ERGIC1, NFYC, UBE2D3, SUZ12, GLIPR1, GPM6B, LRIF1, TAF5L, HERC4, MORC3, MBNL3, UPF2, KRT6B, FLNA, DAG1, TIMM13, BUD31, CUTA, STIM1, EOGT, GEMIN5, GNPAT1, STXBP2, PCCB, EIF3J, CHRAC1, PLAUR, CISD2, BCL7C, TICAM2, KDM1A, PSEN1, STRN, SMARCD2, RARS, RBPJ, LARS, ALDH1A2, CNOT10, UBE2H, TNKS1BP1, PUS7, RPL39, CTSA, MBLAC2, GAR1, RAD1, NOLC1, FGF2, KDELC2, HSPA4L, PEBP1, PNPLA4, GHITM, FAM3C, PGRMC2, RPAP1, NCAPG, PDE12, TFCP2, NKX3-1, L2HGDH, PRKAR2A, ARL5A, CD109, TOMM34, CFL2, AIMP1, MIDN, CDC73, TRIO, PAXBP1, TSPAN14, INTS6, YWHAZ, PRKAR1A, SSX2IP, FAM199X, RAC1, PLS1, SAP30L, MRPS27, TNFAIP2, JUNB, SPCS1, CTNNA1, ASNS, H2AFY, NR3C1, AXL, RING1, CLTA, COL4A2, CNM3, CTNBL1, CNOT9, ATL2, CDK5, PPP2R2A, THOC7, DNMT1, MRPL16, RAB6C, HAX1, ABHD16A, ASB6, GPAM, HDHD5, WDR11, NMD3, IGF2R, ACOT7, RRAGA, INTS7, YARS, FLNB, CORO1B, SUPT5H, KANK2, DIAPH3, FASTKD1, NSA2, FMNL3, CHTOP, STRBP, MARCKS, POLR1B, FNDC3B, CD3EAP, PSAT1, COPS3, DEGS1, OXCT1, PDK1, EIF3A, GMPS, OLR1, SMAD4, CD68, FLT1, CEP41, CIAPIN1, CCDC82, ACTR2, TRAK1, CYP2U1, SLC35F2, ZNF493, HAL, IL17RB, TBC1D14, ZNF254, GABARAPL1, JCHAIN, RAPGEF2, WBP1L, PBRM1, ABCC4, SPECC1, MAT2B, TFPI, EXOC3, PFDN4, HK2, TYSND1, C12orf10, CRAT, PLEKHA5, PACSIN3, F5, SMARCE1, CD81, VAV2, SLC7A1, OBSCN, MAVS, DMD, CARS2, SLC12A4, MRPS34, B4GALT1, KDELC1, PDCD10, NCAPD2, UBA2, ALDH5A1, FUBP3, MYO6, NAA50, MARC2, RIOK2, OSBPL9, DDX10, ATXN10, RAB30, DEK, PHF6, ARL8B, LEMD3, ZNF207, CSE1L, CPT1A, TTC37, MAN1A2, RICTOR, IMPAD1, VPS4B, CLINT1, UBQLN2, RIF1, PNPT1, MRPL18, MAP3K14, ARMC2, LCORL, APAF1, MPP5, RAB11FIP2, NOVA1, RBAK, ARL15, MYO1D, LRRC59, CMSS1, LONP2, MUS81, ITGB4, DDB2, CAT, ATPAF1, TPBG, INTS4, TIMM8A, RBM22, MTFMT, WRB, DDRGK1, GMPPA, EEF1A2, RDH13, CLTC, NOTCH2, CARS, PTMS, CSNK1A1L, LUC7L3, TJP1, FDF1, CDKN2A, AKR1C3, PNPLA8, S100A11, IER3IP1, FSTL1, SLC38A5, ATP6V1H, ITGB5, SRSF2, SLC7A11, ANXA2, DDX17, RAB2A, FOXK1, TMOD3, PSME4, ZNF384, GNAS, SNTB2, TMTC3, SLC30A7, ASPH, INTS8, CPD, EGFR, SRPK2, STAG2, IRF2BP2, TPRKB, VPS36, VCAM1, SMAD3, TTF1, FAM91A1, CEP83, MARF1, CDC40, DCUN1D2, KLHL5, AGO4, HBP1, WWC1, WEE1, GOLT1B, PALD1, THBS1, DBN1, DHCR24, HSD17B7, NSUN5, TPP2, UAP1, OXNAD1, SSSCA1, EEF1E1, PHGDH, CCND1, ALDH3A2, CDK2, SGPL1, TSPAN3, ANPEP, PSME3, AGRN, GNL3L, VANGL1, RTFDC1, WNT5A, TMEM167A, CLIC4, MEST, TRIM24, CDH6, MMS22L, SKIV2L2, CCR9, DR1, RSF1, ANTXR1, SEPT11, HNRNPA3, CXCL8, ZNF83, PHF14, TBC1D8B, INPP5F, ARPC3, KRCC1, FAM177A1, UBTD2, SECISBP2, PAK2, SLC33A1, ZNF28, MCM8, SMARCA4, TCF12, TOMM20, UBQLN1, PDPR, MOV10, FAM120A, FAM96B, FKBP3, STAT3, NEUROG1, EPRS, CDH2, CDH13, ATP13A1, EIF3F, NUP62, GCLC, LSM3, HTRA1, CDK4, EPB41L2, COG2, CCT2, NUCKS1, PRSS21, INTS10, STX5, CIAO1, GLG1, TROVE2, ARGLU1, CALU, BRI3BP, RAD23B, PYGL, MRS2, KIF14, POLR2C, TPD52, MTHFD2, RNF2, LTN1, TMEM33, TNPO1, GSK3B, ADAM10, ERBIN, CCL2, NFKB1, IL6, CD36, RREB1, ZKSCAN5, ZNF611, ZNF273, PDCD4, VPS18, NSD3, MASTL, MYBL1, GATM, E2F2, FAM135A, C3orf18, ARL6IP5, SHANK2, SH3PXD2A, PIK3R1, VHL, PATJ, MMP16, FOS, MAPK14, RAPH1, RAB3B, KLF9, MYC, ITK, IL2, SEL1L, DOCK1, RAD51, THRB, TERF1, ZBTB18, ZNF431, ZBTB38, ZSWIM6, ADD3, S1PR1, CBL, AGTRAP, WNK1, KCTD3, KLHL42, SP1, CHURC1, MEX3C, TWSG1, ZNF492, CCNT2, PIK3CA, DMTF1, CHD7, DCAF10, DDX3Y, CSNK1G2, ZNF714, TADA2B, UBXN2B, ACOX1, ELK4, KCTD5, ANKRD12, HIF1A, ZNF148, NAA16, ETNK2, TRPS1, PEA15, PTN, MX11, SOCS3, ZNF98, ZNF468, ZNF300, ZNF260, ZNF160, ZKSCAN1, YEATS2, XPNPEP1, WDR82, VCIPI1, USP8, UBE2G1, TTC8, NEMP1, TMEM123, TCF4, TAPT1, STRN3, SSU72, SSH2, SLC11A2, SIRT1, SRSF1, KMT5A, SERGEF, RPS20, RGL1, REV1, PTAR1, OSTM1, NFAT5, N4BP1, MKLN1, KPNA5, KIF3A, KCNN3, INPP5A, IFIT5, HMGCS1, HLA-DPA1, GANAB, GALC, SARAF, FGL2, FEZ2, EZH1, ENTPD1, DPY19L1, CREB3L2, CPEB4, CDC37, SWSAP1, BTBD1, AKAP10, ABI2, AAK1, CHD8, AKT1, PHACTR2, XPR1, RAB3IP, KIAA1841, PCCA,</p>
--	--

	RHEBP1, UQCRB, FCAMR, SLC35A1, HHIP, SELENOT, CSRP2, CDKN1B, ZFP36, KANSL1, FITM2, CYP1A1, DENND1B, FAM76A, DOK2, ZNF703, SPRED1, TMEM136, CNOT6, ADAMTS4, MTRNR2L7, MTRNR2L5, PLEKHA2, RORA, ZNF678, UBL3, PRRC1, KLHL28, EEF2, ZNF644, MTRNR2L3, CDV3, MTRNR2L9, CHRDL1, ZNF500, TDRD6, MARVELD1, CNPPD1, FOXE1, TYRP1, MAPK13, SOCS6, RPTOR, TFAM, STAT1, CCND2, CASP3, TBRG1, HOMEZ, NR1H3, PTEN, FBXW7, SAMHD1, CS, GEN1, MTRNR2L1
miR-497-5p	RAF1, RUNX2, IGF1R, MAP2K1, EEF1A1, TCEA1, HIST1H3H, ALDH9A1, DESI2, HIST2H3A, PANK2, ATXN7L3B, BRD1, WEE1, DICER1, HDGF, BCL2, EIF4E, BIRC5, WNT7A, SMURF1, CHEK1, SHOC2, PLEKHA1, CEP55, ZDHHC16, CCND1, C1orf21, AMOTL1, CCND2, TARBP2, MTFR1L, USP15, FCF1, ARIH1, PAGR1, SNTB2, VPS4A, C16orf72, GOSR1, RPS6KB1, NAGP, GALNT1, CCNE1, PNPLA6, ZCCHC3, SOWAHC, UBR3, ZNRF3, YWHAH, B3GNT2, ACTR2, RARB, PI4K2B, CANX, E2F3, PPP1R11, HSPA1B, PIM1, VEGFA, CD2AP, CALU, UBN2, EN2, MAFK, FOXK1, USP42, DMTF1, ZFH4, RAD23B, ZBTB34, RECK, ZNF275, OGT, LUZP1, CHAC1, SCAMP4, PAK2, ENTPD1, SKI, SPRED1, SMAD3, DCTN5, TNFSF9, RASSF2, ATP5G3, TNRC6B, GRAMD2B, CREBRF, PSAT1, PAFAH1B2, RPRD2, PNRC2, CDADC1, AGO4, GPR180, PPM1A, SLC39A9, FAM103A1, RBBP6, TAOK1, SNRBP2, HSPE1-MOB4, MOB4, BZW1, NUP50, FGF2, HSPA4L, RBPJ, TBPL1, FZD6, BAG4, ZNF449, YIPF6, MSL1, ELK4, GABARAPL1, ZNF691, DYNLL2, SRPRB, CDC42SE2, WIPI2, TBRG1, C1orf226, SETD1B, HOXC8, RAB3IP, PPP2R5C, SLCO3A1, CBX2, ZFP28, CHMP4B, GABPA, STRADB, MTMR3, CRIM1, SOCS5, CTDSPL, ITGA2, PIK3R1, PPIL1, CAPZA2, ZNRF2, OCRL, CHIC1, CRKL, BTRC, CDK4, CCND3, CDC25A, SIDT2, ASCC1, DMRT2, TLL1, LUC7L3, ALDH3B1, EFTUD2, CSNK1E, TPM2, ZNF460, FGFR4, DOCK11, ACTR3B, ZNF367, UBE2V1, UBE2Q1, TSC22D2, TOB2, TMEM189-UBE2V1, TMEM189, TM4SF1, TFAP2A, STK38, SRRP1, SIK1, SH3BP4, SEC24A, RNF168, REL, PISD, PDE4D, NR6A1, NFIC, NAA25, LAMC1, RUBCN, IVNS1ABP, IPPK, HOXA3, HEYL, GNB1, GNAL, FURIN, EIF1AX, DYRK3, CPSF7, CDK6, CARD10, AVL9, AKT3, AGO2, ABL2, ABHD2, ABCC6, PRKAR2A, VSIR, PHYHIP, CASKIN1, ZNRF1, CD180, KIAA0895, ORC4, ODF2L, DNAJA1, L2HGDH, ZNF622, ZMAT3, USP53, SYPL1, SRPRA, SREK1, SMAD7, PRICKLE2, LRIG2, KIF5B, FAM122B, E2F7, DDX3X, CDCA4, CDC37L1, ATG9A, ASGR2, ZNF620, HAUS3, YTHDC1, TMEM245, TMEM100, SRSF1, SNX16, SESTD1, RIMS3, RCAN3, PPIG, PLRG1, PLAG1, PHKA1, MYO5A, KIF23, HNRNPDL, CDK1, CCNE2, CBX6, AXIN2, CASK, DMPK, ATAD5, AKR1B10, GPATCH8, ARHGDI, CPEB3, JARID2, CAMSAP1, ATG14, TRIM35, FLCN, NNT, SLC2A3, SBNO1, POM121C, NUFIP2, LAMP2, EFNB2, RPL14, GNAT1, HOXA10, CBX4, PHC3, PDCD1, BAZ2A, APP, ZNF585B, ANAPC13, PRSS21, RALGAPB, GSG1, POLDIP3, AP5Z1, CLSPN, UGT2B4, MAP4K2, CCDC83, DECR1, ZBTB10, YWHAQ, USP48, SALL1, RUNX1T1, RTN4, PNISR, PHLPP2, PAG1, NUCKS1, MKX, MBD4, LRRFIP2, KPNA3, KPNA1, HIGD1A, HCFC2, GRB2, FKBP1A, FBXL20, FASN, CRK, CLIP4, CDK17, CACUL1, C11orf24, ASH1L, AMOT, SLC29A1, OSCAR, MTHFR, FAM229B, EPM2AIP1, ZNF267, SSU72, DNAJC10, ZNF704, YRDC, TPM3, TMEM161B, TM7SF3, TAF13, SZRD1, RNF149, RACGAP1, RAB23, PTPRD, PRKAA1, PRDM4, PLPP3, LURAP1L, KANK1, HIST2H2BE, GPR27, EXT1, CYP26B1, CREBL2, CNKSR3, CA8, BTN3A3, ARHGAP12, OSBPL3, KRT33B, TUBB2A, MSANTD4, LANCL1, HNRNPA2B1, KIAA1456, SLC25A12, DLGAP3, THRAP3, SMDT1, RAPH1, CCNT1, ZNF391, CCDC80, ZBTB16, XKR7, WNK3, VAV2, TGFBR3, RASEF, NCKAP1, MAP3K7, KLHL15, GNG12, FZD9, CMTM4, CCDC88C, ARMC12, AHNK2, ACVR2A, TLK1, UBE2H, TLL5, RIF1, SERBP1, PHF19, LSM11, PLPBP, CLEC2D, PDIA6, N4BP1, TRAK1, ADRA2B, ANKMY1, GPRC5A, C3orf36, BSPRY, ANKRD36, KLHL40, NOTCH2, EIF2B2, CUL3, DCAF17, RS1, GLP2R, FLOT2, HNRNPA1L2, TPM1, NEGR1, MCFD2, HNRNPA1, SLC35E2B, ARHGAP32, RAB15, ADORA3, PPIP5K2, SYNRG, KCNN4, ANLN, Reck, MACC1, PBX3, MTOR, TWIST1, IKBKB, ESRRA, AP2B1, AURKAIP1, BCL2L12, C16orf58, CLU, CLUH, DENND6A, DIAPH1, FBXL18, GATAD2A, HSPA8, IER2, KMT2D, MAP2K3, PLEKHB2, POLR2E, PPP6R3, RNPS1, RPRD1B, SEC61A1, SNCG, WDR13, C21orf62, CARM1, CD274, JPT2, MINK1, RFK, TXNIP, VOPP1, ZNF284
miR-199a-5p	EZH2, IKBKB, CCNL1, LIF, JUNB, MED6, MECP2, ETS2, DDR1, EDN1, MAP3K11, HIF1A, SOX9, SMARCA2, CD44, TMEM54, SMAD4, SULT1E1,

	GPR78, ERBB2, UNG, CAV1, SIRT1, HSPA5, ATF6, ERN1, KL, APOE, DNAJA4, ERBB3, CDH1, PTGS2, RNF11, ZNF544, TFDP2, ZNF844, PANK3, COL19A1, LIN7A, ARHGAP12, CTSC, RND1, NECTIN1, DRAM1, BECN1, MAFB, WNK1, NFKB1, ACVR1B, VEGFA, CDH2, SNAI1, GSK3B, FZD4, WNT2, JAG1, PSG11, PSG3, PIN1, C1orf226, PLEKHG2, PDE11A, SNTB1, SLC38A2, SESN2, RER1, PLXND1, MAP3K9, E2F3, COX15, TSC22D1, CEP120, SLC16A10, POLR2F, RCC1, DYNAP, PAX8, EXTL3, ZNF669, ZNF440, ZNF117, ZNF791, ZNF772, ZNF394, TUBG1, NAA15, DDX19B, RIC8A, C3orf36, SNRNP48, PSAPL1, AKAP17A, PLGRKT, TNFRSF13C, SLC8A1, CSGALNACT1, SERPINH1, TMOD2, DDX3X, ZNF525, ZNF195, ZNF415, ZNF468, ZNF611, ZNF215, ZNF286B, ZFP1, ZNF846, ZNF625, ZNF584, TRIM10, VAV3, OXSR1, PLPP4, A2ML1, RNF115, AGTRAP, NDUFS2, CHRFAM7A, CRIPT, POLA2, GATA6, CDK9, VPS53, PTCD2, SLC26A2, PODXL, ABCC1, TBC1D21, CENPO, CHCHD4, LAX1, SNAP25, HK2, KRAS, SMAD3, ETS1, CCR7, PDE4D, CTGF, TGFB2, PIK3CD, SETD2, LDLR, CLTC, RAB21, OSCP1, PIAS3, PSMD9, CDKN1C, ITGA3, FZD6, MAP4K3, TGFB1, SLC27A1, C16orf58, CSNK2A1, DDI2, GM2A, NAB2, VASP, ZBTB37, QSOX1, ZDHHC9, DDHD1, XRR1
--	--

Supplementary information, Table S5. Experimentally validated target genes of miRNA miR-155-5p, miR-497-5p and miR-199a-5p.

hsa-miR-155-5p		
Term	Gene number (%)	adj p-value
Pathways in cancer	5,8	1,10E-05
PI3K-Akt signaling pathway	4,1	1,10E-02
HTLV-I infection	4	1,90E-04
Hepatitis B	3,2	4,30E-06
FoxO signaling pathway	2,7	1,80E-04
Proteoglycans in cancer	2,7	2,00E-02
Focal adhesion	2,7	2,50E-02
Signaling pathways regulating pluripotency of stem cells	2,5	7,80E-04
TNF signaling pathway	2,4	6,00E-05
RNA transport	2,4	1,70E-02
Influenza A	2,4	1,80E-02
Hepatitis C	2,3	2,60E-03
Transcriptional misregulation in cancer	2,3	2,30E-02
Colorectal cancer	2,2	5,20E-07
T cell receptor signaling pathway	2,2	3,20E-04
Measles	2,2	6,50E-03
Chagas disease (American trypanosomiasis)	2,1	1,00E-03
Osteoclast differentiation	2,1	1,10E-02
AMPK signaling pathway	2	1,20E-02
Ubiquitin mediated proteolysis	2	2,80E-02
hsa-miR-497-5p		
Term	Gene number (%)	adj p-value
Pathways in cancer	7,2	1,60E-05
PI3K-Akt signaling pathway	6,5	1,80E-05
MicroRNAs in cancer	4,8	1,20E-03
MAPK signaling pathway	4,1	4,10E-03
Viral carcinogenesis	3,9	1,30E-03
Focal adhesion	3,9	1,30E-03
Cell cycle	3,7	2,50E-05
Insulin signaling pathway	3,5	2,50E-04
Signaling pathways regulating pluripotency of stem cells	3,5	2,70E-04
Hepatitis B	3,5	3,40E-04
Proteoglycans in cancer	3,5	5,90E-03
HTLV-I infection	3,5	3,90E-02

Epstein-Barr virus infection	3,3	9,30E-03
Ras signaling pathway	3,3	3,50E-02
Hippo signaling pathway	3	4,00E-03
Small cell lung cancer	2,8	2,20E-04
Prostate cancer	2,8	2,30E-04
FoxO signaling pathway	2,8	4,50E-03
Acute myeloid leukemia	2,6	3,10E-05
Chronic myeloid leukemia	2,6	2,10E-04
hsa-miR-199a-5p		
Term	Gene number (%)	adj p-value
Pathways in cancer	12	7,40E-06
HTLV-I infection	9,6	1,20E-05
MicroRNAs in cancer	7,8	1,90E-03
Proteoglycans in cancer	7,2	5,50E-04
Pancreatic cancer	6,6	5,20E-07
Signaling pathways regulating pluripotency of stem cells	6	8,60E-04
Hippo signaling pathway	6	1,40E-03
Hepatitis B	5,4	4,40E-03
Adherens junction	4,8	7,60E-04
Chronic myeloid leukemia	4,8	6,60E-04
FoxO signaling pathway	4,8	1,30E-02
Colorectal cancer	4,2	1,50E-03
Prostate cancer	4,2	8,00E-03
HIF-1 signaling pathway	4,2	1,20E-02
TNF signaling pathway	4,2	1,50E-02
Cell cycle	4,2	2,80E-02
Non-alcoholic fatty liver disease (NAFLD)	4,2	5,60E-02
B cell receptor signaling pathway	3,6	1,40E-02
Small cell lung cancer	3,6	3,00E-02
Melanogenesis	3,6	5,10E-02

Supplementary information, Table S6. Pathway enrichment analysis on miR-155-5p, miR-497-5p and miR-199a-5p experimentally validated targets (top 20 KEGG pathways are shown).

EVs			MSCs		
Order of inclusion by Ranking-PCA	Variable	loadings on PC1	Order of inclusion by Ranking-PCA	Variable	loadings on PC1
1	hsa-miR-193b-3p	0.078085	1	hsa-miR-146b-3p	0.074598
2	hsa-miR-142-5p	0.065747	2	hsa-miR-143-5p	-0.07444
3	hsa-miR-21-5p	-0.07851	3	hsa-miR-28-5p	0.074518
4	hsa-miR-222-3p	-0.07351	4	hsa-miR-26b-3p	-0.07445
5	CALM	-0.07058	5	hsa-miR-328-3p	-0.07424
6	TPM2	-0.07971	6	hsa-miR-148a-5p	-0.07403
7	hsa-miR-224-5p	-0.06595	7	hsa-miR-146b-5p	0.073847
8	hsa-miR-143-3p	-0.0804	8	hsa-miR-125b-2-3p	-0.07396
9	hsa-miR-185-5p	-0.05751	9	hsa-let-7f-5p	0.074328
10	VIME	-0.08363	10	hsa-miR-424-3p	0.073985
11	hsa-miR-629-5p	0.055107	11	hsa-miR-874-3p	-0.07424
12	hsa-miR-126-3p	0.082491	12	hsa-miR-382-5p	0.074017
13	hsa-miR-221-5p	-0.06161	13	hsa-let-7i-5p	0.074116
14	hsa-miR-132-3p	0.066751	14	hsa-miR-1276	-0.07221
15	hsa-miR-485-5p	-0.05812	15	hsa-miR-32-5p	0.073731
16	MOES	-0.07947	16	hsa-miR-149-5p	-0.07415
17	hsa-miR-199a-5p	-0.05395	17	hsa-miR-28-3p	0.073542
18	hsa-let-7a-5p	-0.07549	18	hsa-let-7a-5p	0.073508
19	MED6	0.080234	19	hsa-miR-155-5p	0.073754
20	hsa-miR-23b-3p	0.048775	20	hsa-miR-92a-3p	0.07238
21	hsa-miR-196a-5p	-0.08271	21	hsa-miR-99a-5p	0.073624
22	hsa-miR-146b-5p	0.052877	22	hsa-let-7b-3p	-0.07447
23	hsa-let-7i-5p	-0.07156	23	hsa-miR-574-3p	0.074337
24	APOB	0.063557	24	hsa-miR-3909	-0.07419
25	hsa-miR-125b-5p	-0.06961	25	hsa-miR-1296-5p	-0.0737
26	A2MG	0.060184	26	hsa-miR-7-5p	0.074119
27	hsa-miR-31-3p	0.066542	27	hsa-miR-196a-5p	0.07339
28	hsa-miR-16-2-3p	-0.05081	28	hsa-miR-1287-5p	-0.07365
29	CO4A	0.079064	29	hsa-miR-30e-3p	-0.07272

Supplementary Information, Table S7. Loadings on PC1 of the first 200 variables included by Ranking-PCA merging miRNA and proteomic data for both EVs and MSCs. Variables are listed in order of inclusion by Ranking-PCA.

Protein	Primary Antibody	Primary Antibody dilution used	Secondary Antibody	Secondary Antibody dilution used
CD44 molecule	CD44 GeneTex (GTX628472)	1:500	Anti-Mouse Santa Cruz Biotechnology (sc-516102)	1:2000
CD63 molecule	CD63 GeneTex (GTX17441)	1:500	Anti-Rabbit Santa Cruz Biotechnology (sc-2004)	1:5000
Endoglin	CD105 GeneTex (GTX100508)	1:500	Anti-Rabbit Santa Cruz Biotechnology (sc-2004)	1:5000
Galectin-3 binding protein	Mac-2BP Santa Cruz Biotechnology (sc-374541)	1:100	Anti-Mouse Santa Cruz Biotechnology (sc-516102)	1:1000
Melanoma cell adhesion molecule	CD146 GeneTex (GTX108777)	1:500	Anti-Rabbit Santa Cruz Biotechnology (sc-2004)	1:5000
Moesin	Moesin Cell Signaling (#3150)	1:1000	Anti-Rabbit Santa Cruz Biotechnology (sc-2004)	1:5000

Pentatraxin3	Ptx3 Santa Cruz Biotechnology (sc-373951)	1:200	Anti-Mouse Santa Cruz Biotechnology (sc-516102)	1:1000
S-100A6	Calcyclin Santa Cruz Biotechnology (sc-271396)	1:200	Anti-Mouse Santa Cruz Biotechnology (sc-516102)	1:1000

Supplementary information, Table S8. List of antibodies used for western blotting validation